

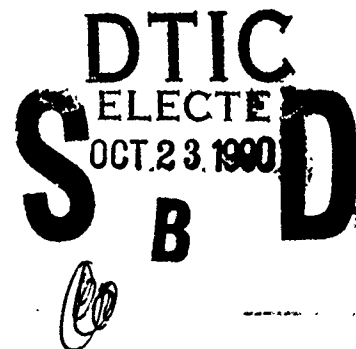
GL-TR-90-0130  
ENVIRONMENTAL RESEARCH PAPERS, NO. 1064

Modeling the Variation of Cloud Cover With  
View Angle Using Space Shuttle Cloud Imagery

J. W. SNOW



10 May 1990



Approved for public release; distribution unlimited.



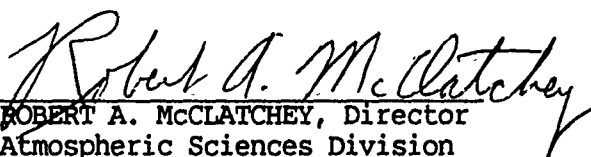
ATMOSPHERIC SCIENCES DIVISION PROJECT 6670  
**GEOPHYSICS LABORATORY**  
HANSCOM AFB, MA 01731-5000

This report has been reviewed by the ESD Public Affairs Office (PA) and is releasable to the National Technical Information Service (NTIS).

"This technical report has been reviewed and is approved for publication"

FOR THE COMMANDER

  
DONALD D. GRANTHAM, Chief  
Atmospheric Structure Branch

  
ROBERT A. McCLATCHEY, Director  
Atmospheric Sciences Division

Qualified requestors may obtain additional copies from the Defense Technical Information Center. All others should apply to the National Technical Information Service.

If your address has changed, or if you wish to be removed from the mailing list, or if the addressee is no longer employed by your organization, please notify AFGL/DAA, Hanscom AFB, MA 01731. This will assist us in maintaining a current mailing list.

Do not return copies of this report unless contractual obligations or notices on a specific document requires that it be returned.

# REPORT DOCUMENTATION PAGE

Form Approved  
OMB No. 0704-0188

Public reporting burden for this collection of information is estimated to average 1 hour per response, including the time for reviewing instructions, searching existing data sources, gathering and maintaining the data needed, and completing and reviewing the collection of information. Send comments regarding this burden estimate or any other aspect of this collection of information, including suggestions for reducing this burden, to Washington Headquarters Services, Directorate for Information Operations and Reports, 1215 Jefferson Davis Highway, Suite 1204, Arlington, VA 22202-4302, and to the Office of Management and Budget, Paperwork Reduction Project (0704-0188), Washington, DC 20503.

1. AGENCY USE ONLY (Leave blank)		2. REPORT DATE 10 May 1990	3. REPORT TYPE AND DATES COVERED Scientific Interim	
4. TITLE AND SUBTITLE MODELING THE VARIATION OF CLOUD COVER WITH VIEW ANGLE USING SPACE SHUTTLE CLOUD IMAGERY			5. FUNDING NUMBERS PE - 62101F PR - 6670 TA - 09 WU - 14	
6. AUTHOR(S)  J. W. SNOW				
7. PERFORMING-ORGANIZATION NAME(S) AND ADDRESS(ES)  Geophysics Laboratory (LYA) Hanscom Air Force Base, MA 01731-5000			8. PERFORMING ORGANIZATION REPORT NUMBER  GL-TR-90-0130 ERP, No. 1064	
9. SPONSORING/MONITORING AGENCY NAME(S) AND ADDRESS(ES)			10. SPONSORING/MONITORING AGENCY REPORT NUMBER	
11. SUPPLEMENTARY NOTES				
12a. DISTRIBUTION / AVAILABILITY STATEMENT  Approved for public release  Distribution unlimited			12b. DISTRIBUTION CODE	
13. ABSTRACT (Maximum 200 words)  This report documents the development of numerous elementary cloud cover models and evaluates the capability of each by comparison with actual data. The data are measurements of apparent cloud cover as a function of view angle obtained from space shuttle cloud photographs. Using these data a physically realistic model for cumuliform cloud fields is obtained. The model permits the determination of actual cloud cover from a single measurement of apparent cloud cover at a known view angle, at least for the single-layer totally opaque clouds considered in this research. Additionally, the model is used to specify the probability of cloud-free viewing from space through such cloud fields. These probabilities are compared with similar ones obtained from other models of cloud-free line-of-sight commonly in use.				
14. SUBJECT TERMS Cloud cover, apparent cloud cover, sky cover, view angle, cumuliform cloud cover models, cloud-free line-of-sight, space shuttle cloud photographs			15. NUMBER OF PAGES 60	
			16. PRICE CODE	
17. SECURITY CLASSIFICATION OF REPORT  UNCLASSIFIED	18. SECURITY CLASSIFICATION OF THIS PAGE  UNCLASSIFIED	19. SECURITY CLASSIFICATION OF ABSTRACT  UNCLASSIFIED	20. LIMITATION OF ABSTRACT  SAR	

## Preface

The data which has made this research possible originated from series of cloud photographs taken on-orbit by astronauts Gary E. Payton, USAF, David C. Hilmers, USMC, and Steven A. Hawley, NASA. Their superlative efforts are commended. The original design and implementation of the space shuttle experiment which produced the cloud imagery used in this report were ably accomplished by Edward M. Tomlinson, USAF, and Hulbert L. Ferger, The Aerospace Corporation. For the painstaking processing and printing of these film records, sincere thanks are extended to Robert J. Maulfair, The Aerospace Corporation. The digitization and computer analysis of the Cape Canaveral, Florida and the Maui, Hawaii series of photographs were accomplished by Chase Consulting, Inc., San Diego, CA, as part of a Small Business Innovative Research, Phase II contract. Appreciation is expressed for review of the manuscript to Donald D. Grantham, Irving I. Gringorten, Crystal L. Barker Schaaf and Paul Tattelman, Geophysics Laboratory, Air Force Systems Command.



Accession For	
NTIS GRA&I	<input checked="checked" type="checkbox"/>
DTIC TAB	<input type="checkbox"/>
Unannounced	<input type="checkbox"/>
Justification	
By	
Distribution/	
Availability Codes	
Dist	Avail and/or Special
A-1	

## Contents

1. INTRODUCTION	1
2. QUANTIFICATION OF CLOUD AMOUNT	2
3. CLOUD COVER MODELS	4
4. MODEL CHARACTERISTICS	9
5. DATA	11
6. MODEL TESTING	12
7. APPLICATION TO SATELLITE CLOUD COVER MEASUREMENTS	17
8. APPLICATION TO CLOUD-FREE VIEWING	21
9. SUMMARY	26
References	27
Appendix A: Intercomparison of the SRI and MOE Pcflos Models	39
Appendix B: Consideration of Shallow-Angles	43

## Illustrations

1. Cloudiness quantifications; 29  
 $S$  - apparent cloud cover,  $C$  - cloud cover,  
 $G$  - ground cover,  $N$  - sky cover.  $\zeta$  is  
view angle. Heavy line segments depict  
areas masked from view by cloud.
2. View angle  $\zeta$  and associated elements 29  
involved in observing a surface target from an  
orbital vantage point.
3. Simple examples of cloud population 30  
models, Type A-cube and Type B-sphere, used to  
derive the apparent cloud cover  $S$  as a function  
of the view angle  $\zeta$ . Heavy horizontal segments  
signify  $S$ .  $L$  is the recurrence interval, the  
linear dimension of one complete cloud/no-cloud  
cycle. Cloud cover  $C$  is  $y^2/L^2$  for the cube,  
 $(\pi/4)y^2/L^2$  for the sphere.  $S_c = y(y+x)/L^2$ ,  
 $x = z \tan \zeta$  and  $y = z$  for the cube. Therefore,  
 $S_c = C(1 + \tan \zeta)$ .  $S_s = (\pi/4)(y^2/L^2) \sec \zeta$ ,  
or  $S_s = C \sec \zeta$ . The critical view angle  $\zeta_c$   
is the smallest value of  $\zeta$  for which two clouds  
mask the same portion of the surface.
4. Apparent cloud cover, shaded horizon- 30  
tal area, resulting from two idealized clouds  
viewed from angle  $\zeta$ : hemisphere of radius  $r$ ,  
hemi-ellipsoid of major axis  $a$  and minor axis  $b$ .  
The half toward the direction of view masks as a  
hemi-disk of radius  $r$  or  $b$ , respectively. The  
half away from the direction of view masks as  
the hatched planes.
5. Derivation of the apparent cloud cover 31  
for the domed cylinder cloud morphology using the  
technique of portions. The half toward the direc-  
tion of view masks as a hemi-disk of radius  $r=y/2$ ,  
the vertical extent of cylinder as a rectangle  $zy$ ,  
and the domed top as the hatched plane. Shaded  
horizontal area is the total area masked from  
view,  $C \sim \pi y^2/4$ .
6. Analysis technique for apparent cloud 32  
cover determination. The same area,  $A_{total}$ , is  
identified in each image (inside edge of white  
quadrangles) and measurement is made of the  
portion occupied by clouds,  $A_{cloud}$ . Apparent  
cloud cover  $S = A_{cloud}/A_{total}$ . The land is a  
portion of the state of Baja California Sur,  
Mexico. The view angle at the center of each

6. (continued)  
of the 3 images is determined photogrammetrically and is shown in the upper right corner. (Inverted numbers in upper left indicate time.) The photographs were taken by astronaut Gary E. Payton, USAF. Additional details are contained in Table 2.

7. Apparent cloud cover  $S$  as a function of view angle  $\zeta$  for cumuliiform clouds. Data from analysis of space shuttle photographs are plotted as open circles. Heavy solid curve is the cumuloid model Eq (15), light solid curve is the domed cylinder model Eq (14), light broken is the sphere model Eq (12). 33

7a. Baja California Sur, Mexico. 33

7b. Offshore of Cape Canaveral, Florida. 33

7c. Vicinity of Cape Canaveral, Florida. 34

7d. Maui, Hawaii. 34

7e. Northeastern Dominican Republic. 34

8. Probability of cloud-free viewing from space  $P(\%)$  as a function of elevation angle  $\theta$  or view angle  $\zeta$  using the cumuloid model. Cloud cover  $C$  (tenths  $\times 10$ ) is the parameter. The right ordinate expresses  $P(90) = 1 - S(0)$ . 35

9. Probability of cloud-free line of sight, cflos--broken curves, and cloud-free viewing from space, cfvfs--solid curves, as functions of elevation angle  $\theta$  or view angle  $\zeta$ . Probability values  $P$  in percent. Cloud cover (tenths  $\times 10$ ) is the parameter. SRI formulation used for cflos and the CMD model used to compute cfvfs values. Conversion from cloud cover to sky cover accomplished using Eq (20). (see Appendix A for  $N$ -values.) 36

10. Probability of cloud-free line of sight, cflos--broken curves, and cloud-free viewing from space, cfvfs--solid curves, as functions of elevation angle  $\theta$  or view angle  $\zeta$ . Probability values  $P$  in percent. Cloud cover (tenths  $\times 10$ ) is the parameter. MOE model used for cflos and the CMD model used to compute cfvfs values. 37

A1. Intercomparison of Pcflos models:  
solid curves - SRI model (modified Lund/Shanklin),  
broken curves - MOE model (Mulamaa-Okhvril-Epik,  
also called Eastern European or Russian model).  
P is probability in percent,  $\theta$  is elevation  
angle,  $\zeta$  is view angle,  $\theta + \zeta = \pi/2$ . The cloud  
amount parameter is cloud cover C, in tenths  
 $\times 10$ . At zenith ( $\theta = \pi/2$ ),  $P = 10 \times (10 - C)$ .  
Conversion from sky cover to cloud cover accom-  
plished using Eq (20). All curves converge to  
zero at  $\theta = 0$ .

41

B1. Probability of cloud-free viewing  
from space (%) as a function of elevation angle  $\theta$   
or view angle  $\zeta$  using the cumuloid shallow-  
angle CDS model. Cloud cover C (tenths  $\times 10$ )  
is the parameter. The right ordinate expresses  
 $P(90) = 1 - S(0)$ .

47

B2. Probability of cloud-free line of  
sight, cflos--broken curves, and cloud-free  
viewing from space, cfvfs--solid curves, as  
functions of elevation angle  $\theta$  or view angle  
 $\zeta$ . Probability values P in percent. Cloud  
cover (tenths  $\times 10$ ) is the parameter. SRI  
formulation used for cflos and the CDS model  
used to compute cfvfs values. Conversion from  
cloud cover to sky cover accomplished using  
Eq (20). (See Appendix A for N-values.)

48

B3. Probability of cloud-free line of  
sight, cflos--broken curves, and cloud-free  
viewing from space, cfvfs--solid curves, as  
functions of elevation angle  $\theta$  or view angle  
 $\zeta$ . Probability values in percent. Cloud  
cover (tenths  $\times 10$ ) is the parameter. MOE  
model (see text) used for cflos and CDS model  
used to compute cfvfs values.

49



## Tables

1. Models of Apparent Cloud Cover as a Function of View Angle	6
2. Space Shuttle CLOUDS Photographic Series of Single-Layer Cumuliform Clouds	12
3. Comparative Cloud cover Models	14
4. Space Shuttle Cloud Photograph Data Sets and Cloud Cover Values Estimated Using Cumuloid Model With $\nu = (1-C)^2$ .	20
5. Probabilities of Cloud-Free Viewing From Space (%), Pcfvfs, Determined Using the Cumuloid Clear-Viewing (CMD) Model	22
6. Probabilities of Cloud-Free Line-of-Sight and of Cloud-Free Viewing From Space (%), Pcflos/Pcfvfs, Determined Using the SRI Model for Pcflos and the Cumuloid Clear-Viewing Model for Pcfvfs	24
7. Probabilities of Cloud-Free Line-of-Sight and of Cloud-Free Viewing from Space (%), Pcflos/Pcfvfs, Determined Using the MOE Model for Pcflos and the CMD Model for Pcfvfs	25
A1. Comparative Probabilities of Cloud-Free Line-of-Sight Determined Using the SRI Model and the MOE Model. Entries are SRI(%) / MOE(%)	39

## MODELING THE VARIATION OF CLOUD COVER WITH VIEW ANGLE USING SPACE SHUTTLE CLOUD IMAGERY\*

### 1. INTRODUCTION

Technological advances in DoD systems and increasing sophistication and refinement in battlefield management are very often limited by the environment, particularly the variably cloudy atmosphere. One troublesome aspect of clouds is the fact that the portion of a horizontal surface which they block from view increases as the angle at which viewing is done departs from nadir. The probability of cloud-free viewing from a location on the Earth's surface vertically upward to space is given by the fraction of the atmosphere which is clear, that is,  $(1 - C)$ , where  $C$  is the cloudy fraction and is commonly called the cloud cover. The same expression gives the probability of cloud-free viewing from space to a nadir point on the Earth's surface. However, what is the probability at angles other than vertically upward or vertically downward? The 3-dimensionality of clouds must implicitly or explicitly be considered in order to provide the answer.

In this report, photographic data of cumuliform cloud scenes taken during 1984 and 1985 space shuttle missions are used to specify the apparent increase in cloud cover with the angle at which the clouds are viewed. These data allow the testing of various idealized cloud cover models that make use of clouds having simple geometric shapes. An optimum cloud cover model for single-layer, totally opaque cumuliform clouds is developed. The model is applied to the problem of estimating  $C$  when only an off-nadir measurement of cloud amount is available. It is also used to specify the probability of cloud-free viewing as a function of angle for any amount of cumuliform cloud cover.

(Received for publication 10 May 1990.)

---

\* This is the technical report which is referred to as "Variation of Cumuliform Cloud Amount with View Angle" in Minnis (1989).

## 2. QUANTIFICATION OF CLOUD AMOUNT

In the strict sense, "cloud cover"  $C$  is defined as the fraction of a given area that is overlaid in the local normal direction by clouds; its range is  $0 < C < 1$ . It is the portion of the Earth's horizontal surface masked by the vertical projection of clouds. As seen from below, cloud cover is the fraction of an imagined horizontal surface located above all clouds that is masked by the projection of clouds in the direction perpendicular to that surface. Cloud cover is the fundamental physical quantity specifying cloud amount that is needed in energy budget computations, dynamic modeling and bulk transmissivity studies involving the atmosphere.

Whenever viewing is done through a cloudy atmosphere at any angle other than the local normal, upward or downward, the quantification of cloudiness is larger than  $C$ . Cloud cover assessments can be made from single points that are variously located on the Earth's surface, within the cloudy atmosphere or above all possible clouds. Common examples are illustrated in Figure 1. In such cases, angles far different from the local normal, may be involved. Therefore, single point evaluations typically result in overestimations of the amount of cloud cover. The physical reasons are: (1) the divergence of tangent rays when the point of observation is relatively close to the clouds, (2) the fact that cloud surfaces, which are vertical and therefore do not contribute to  $C$ , cannot be distinguished from surfaces that are horizontal, and (3) the increased path length with increased angle off-normal for viewing through layers containing clouds of non-uniform opacity. In the analytical portions of this report, only the second of these is explicitly considered, that is, the clouds are far enough away from the point of observation so that the tangent rays are essentially parallel and the clouds are considered totally and uniformly opaque.

A meteorological technician observing from the surface is instructed to evaluate "sky cover" as the fraction of a hypothetical sky dome masked from

view by clouds. The symbol  $N$  is often used to indicate this fraction. The hypothetical sky dome intersects the surface at the observer's horizon. Generally,  $N > C$ , yet it is not as biased an estimate of  $C$  as would be the case if the instructions were to project clouds onto other conceivable hypothetical surfaces such as the one above all clouds and parallel to the Earth's surface. The effect of diverging tangent rays can also contribute to  $N > C$ .

In aviation meteorology, cloud amount is called "ground cover"  $G$ , defined as the fraction of a given area on the Earth's surface unseen because of clouds. Except for the case where the given area is vertically downward and the point of observation is far enough above all clouds to result in parallel rays,  $G > C$ . For aircraft operations it is the needed quantity; areas unseen from aircraft due to the vertical extent of clouds (or diverging tangent rays) are as blocked from surveillance as those hidden by the true horizontal extent of clouds.

If the point of assessment is significantly above all possible clouds, the tangent rays are essentially parallel and an appropriate term, as depicted in Figure 1, is "apparent cloud cover"  $S$ . Commonly such assessments are made using meteorological satellites and therefore "satellite cloud cover" can also be used to describe the quantity  $S$ . In this report the terms apparent cloud cover and satellite cloud cover are entirely equivalent and both are indicated by the symbol  $S$ . Analytical expressions for the relationship  $S > C$  are developed in Section 3; tests and applications are then carried out.

The extent to which  $S$  exceeds  $C$  is a function of the departure from vertical of the angle at which the clouds are viewed. It is necessary to define this angle in a manner that is independent of the height and range of the point of observation from which a cloud scene is viewed. In Figure 2 the "view angle"  $\zeta$  is the appropriate angle whereas  $\tau$  the "tilt angle", also known as the satellite "scan angle", is not since it is dependent on the observation point. It can now be stated that  $S(\zeta) > S(0) = C$ .

The relationship  $S(\zeta)$  is the topic of this report. It is of interest for various reasons among them being the fact that the assessment of  $C$  on a global scale can only be accomplished using meteorological satellite platforms whose sensors function throughout the range  $0 < \tau < 75^\circ$ , meaning  $0 < \zeta < 90^\circ$ . The relationship is not easily generalized because no two cloud scenes are alike. Each cloud scene may not only have its own cloud amount but also the clouds themselves differ in size, shape, base-height, thickness, spacing and opacity from one cloud scene to another. In view of these many variables and the enormous number of possible combinations, a stochastic approach to the general problem is probably required. But stochastic simulations must conform to analytical models for situations which are simple enough to be handled deterministically. The analytical solution of  $S(\zeta)$  which is here developed can be used as such a conformity check, at least for the basic situation of single-layered, totally opaque cumuliform clouds. Its development is considered by Snow et al (1986) and is covered in some detail below. It is emphasized that only totally opaque clouds are explicitly considered in this report. The phenomenon of  $S(\zeta)$  for optically thin clouds will be dealt with in a later report.

### 3. CLOUD COVER MODELS

A field of clouds consists of a myriad of individual clouds, no two of which are identical. However, each cloud has certain characteristics similar to all others in the field, for example, all may have rather flat bases, rounded tops, vertical sides, somewhat circular horizontal cross-sections, etc. In addition, certain ensemble characteristics of the cloud field are fixed; the most evident one being the amount of cloud,  $C$ . An actual cloud field can be represented by an idealized cloud population which preserves the characteristics required for a specific purpose but which obviates consideration of the wide variability present in other characteristics of the cloud field not needed for that purpose. As an example, if cloud amount is being modeled, it is not necessary to consider the number of clouds, the individual cloud sizes or the dimensions of clear spaces.

The simple idealized cloud populations employed in this report are made up of regularly spaced single-layered clouds all having the same size and shape. The ensemble characteristic of the real cloud field which must be preserved in these idealizations is  $C$ . What varies among these models is cloud morphology. The simplest possibilities are horizontal 2-dimensional shapes, e.g. squares or circles, referred to as Type 2D in Table 1. For these unrealistic cloud morphologies  $C = S \neq f(\zeta)$ . There are two genera of simple 3-dimensional cloud morphologies: Type A -- those having clouds of constant vertical thickness  $z$ , and Type B -- those with clouds having variable  $z$ , e.g. rounded-tops. The distinction can be seen in the form of the  $S$  versus  $\zeta$  relationship. Type A has  $S \sim \tan \zeta$ , whereas Type B has  $S \sim \sec \zeta$ . The simplest cases of each type are cubes for Type A and spheres for Type B, which are detailed in Figure 3. Mathematically, the  $S(\zeta)$  relationships for these simplest morphologies are:

$$S_c(\zeta) = C(1 + \tan \zeta) \quad (1)$$

$$S_s(\zeta) = C \sec \zeta \quad (2)$$

where the meaning of the subscripts is cube model and sphere model, respectively.

More generally, the thickness of the idealized clouds,  $z$ , is allowed to be different from the horizontal dimension  $y$ . This is most readily accomplished by parameterizing the cloud thickness in terms of horizontal dimension, namely  $\beta = z/y$ , the ratio of maximum vertical dimension of the cloud to the horizontal dimension in the plane in which  $\zeta$  is measured.  $\beta$  is here referred to as the thickness parameter and in some of the references as the height-to-width ratio.

Introduction of  $\beta$  into Eq (1) results in the more realistic rectangular solid model

$$S_r(\zeta) = C(1 + \beta \tan \zeta) \quad (3)$$

which was first published by Lund in 1965. (It should be noted that "viewing angle" as used by Lund (1965) is  $(90^\circ - \zeta)$  in present notation.) Table 1

Table 1. Models of apparent cloud cover as a function of view angle

	Individual Cloud Morphology	C Cloud Cover	S( $\zeta$ ) Apparent Cloud Cover	$\beta$ Thickness Parameter
Type 2D, z=0	Square	$y^2/L^2$	C	none
	Disk	$\pi/4 y^2/L^2$	C	none
Type A z constant	Cube	$y^2/L^2$	$C(1 + \tan \zeta)$	1
	Rectangular Solid	$y^2/L^2$	$C(1 + \beta \tan \zeta)$	z/y
	Cylinder (base horizontal)	$\pi/4 y^2/L^2$	$C(1 + \frac{4}{\pi} \beta \tan \zeta)$	z/y
Type B z variable	Sphere	$\pi/4 y^2/L^2$	$C \sec \zeta$	1
	Ellipsoid	$\pi/4 y^2/L^2$	$C\beta \frac{\sec \zeta}{R(\psi)}$	a/b
	Hemisphere (base horizontal)	$\pi/4 y^2/L^2$	$C \frac{1}{2} (1 + \sec \zeta)$	1/2
	Hemi-Ellipsoid (base horizontal)	$\pi/4 y^2/L^2$	$C(\frac{1}{2} (1 + 2\beta \frac{\sec \zeta}{R(\psi)}))$	a/2b
	Domed Cylinder (base horizontal)	$\pi/4 y^2/L^2$	$C(\frac{1}{2} (1 + \sec \zeta + \frac{8}{\pi} \beta_c \tan \zeta))$	z/y+1/2

- l. - recurrence interval (see Figure 3)  
 y - maximum horizontal cloud dimension  
 z - maximum vertical cloud dimension  
 r - radius  
 a - semi-axis in the vertical direction  
 b - semi-axis in the horizontal direction  
 $R(\psi) = (\sin^2 \psi + \beta^2 \cos^2 \psi)^{1/2}$ ,  $\psi = \zeta + \delta$  (see Figure 4)

summarizes the models so far discussed as well as other possibilities. The rectangular solid model is the first with flexibility regarding the thickness parameter although  $z$  is constant across the cloud's extent since it is Type A.

Proceeding to more realistic models, it is common observation that cumulus clouds have flattened bases and bulbous tops. A model which incorporates both variable thickness and flattened base is the hemisphere. The equation for this cloud morphology is

$$S_h(\zeta) = \frac{C}{2} (1 + \sec \zeta) \quad (4)$$

The development is shown in Figure 4 where the totality of the cloud is treated by portions. The half toward the direction of view acts like half of a horizontal disk and contributes a constant amount to  $S$  for all values of  $\zeta$ , specifically  $C/2$ . The away-half interrupts the view as a halved hemisphere, that is, a quarter of a sphere which has its plane vertical surface perpendicular to the plane in which  $\zeta$  is measured. The thickness parameter for the quarter-sphere, like the whole sphere, is  $\beta = 1$  (versus that for the whole hemisphere which is  $1/2$ ). That two terms appear in Eq (4) is thus explained. Multiplication of the cross-sectional area of the away-half which is perpendicular to the direction of view by  $\sec \zeta$  gives the portion of a horizontal surface which is masked by the quarter-sphere.

The hemisphere morphology more closely resembles real cumulus clouds and further, the hemi-ellipsoid model adds flexibility in the thickness parameter which is not available in the hemisphere model. In fact the hemisphere model is a special case of the hemi-ellipsoid model. For an ellipsoid of revolution with its major axis pointing in the vertical, the apparent cloud cover as a function of view angle is

$$S_e(\zeta) = C\beta \frac{\sec \zeta}{R(\psi)} \quad (5)$$

where  $\beta$  is the ratio of major over minor axis  $a/b$  and  $R(\psi)$  is given at the bottom of Table 1. The sphere model is the special case of  $a=b$ , or  $\beta=1$ .



The development of Eq (5) can be understood as the extension of the hemi-ellipsoid model shown in Figure 4. The derivation is accomplished by portions, as with the hemisphere, and the resulting two-term equation is

$$S_l(\zeta) = \frac{C}{2} \left( 1 + 2\beta \frac{\sec \zeta}{R(\psi)} \right) \quad (6)$$

With Eq (5) and Eq (6) flexibility with respect to the thickness parameter is gained. Further development of the ellipsoid models is not included here but either might be used if  $\beta$  were known.

The parameter  $\beta$  is an ensemble characteristic of the cloud population. It is not necessarily the height-to-width ratio of any individual cloud or even the average for all clouds in the population. While being related to these, it is primarily a model vertical extent parameter which must somehow be dealt with.

In addition to variable thickness and flattened bases, more realistic morphologies can be studied using the technique of linear combination of portions which is applied in the hemisphere case. The morphology of typical cumulus clouds can be described as that of a domed cylinder. The simplest domed cylinder consists of a hemisphere of radius  $r$  positioned on top of a cylinder of diameter  $y = 2r$  and of height  $z$ . From Figure 5 the apparent cloud cover for domed cylinders is

$$S_m(\zeta) = \frac{C}{2} (1 + \sec \zeta + B \tan \zeta) \quad (7)$$

where  $B$  is the thickness parameter of the cylindrical base portion of the cloud  $\beta_c$  multiplied by  $8/\pi$ , specifically  $B = \frac{8}{\pi} \beta_c$ . (The thickness parameter for the entire domed cylinder is  $\beta = \beta_c + 1/2 = z/y + 1/2$ .)

Other combinations are easily derived, for example, a cylinder topped by a hemi-ellipsoid. However when the models are fitted to actual data, such added complexity is not warranted. The domed cylinder model Eq (7), is the simplest model having both variable  $z$  across the idealized cloud (the feature of Type B) and flexibility in regard to the thickness parameter (through  $\beta_c$ ). In a more

general sense and irrespective of any particular geometric shape for clouds, the presence of a  $\sec \zeta$  term accounts for the increased path length and therefore increased likelihood of a ray intersecting with a cloud within a cloudy layer and the presence of a  $\tan \zeta$  term accounts for the horizontal projection of the vertical extent of clouds.

#### 4. MODEL CHARACTERISTICS

Before proceeding to the testing of the models using actual data, two important characteristics which any useful cloud cover model must have are considered. The first is continuity, the second is compensation for multiple-masking.

Continuity means that at the vertical angle  $\zeta = 0$  (the nadir angle as seen from above), the rate of change of apparent cloud cover  $dS/d\zeta$  must be continuous and, in fact, must be equal to zero. This is because at  $\zeta = 0$ ,  $S$  attains its minimum value which is  $C$ , the cloud cover itself. Implicitly, therefore,  $S$  must also be an even function of  $\zeta$  since  $S$  increases as  $\zeta$  increases from zero in either a positive or negative sense. Any Type B model in Table 1 (except the last) has this characteristic without imposing additional restrictions on  $\beta$ . The last model in Table 1, the domed cylinder as expressed in Eq (7), reduces to the hemisphere model to meet the requirement unless the allowance is made  $B = f(\zeta)$ , more specifically  $B$  must equal an odd  $f(\zeta)$  since  $\tan \zeta$  is itself odd. This possibility will be considered in detail in Section 6. The only way Type A models can meet this requirement (as carrying out the differentiation will confirm) is for  $\beta = 0$  which degenerates them into the useless 2-dimensional horizontal square or disk,  $S(\zeta) = C \neq f(\zeta)$ . Therefore, it can be concluded that all Type A models are inherently suspect near nadir, that is, at low values of  $\zeta$ .

Multiple-masking means that a portion of a horizontal surface concealed from view by one particular cloud is also blocked from view by another cloud.

As  $\zeta$  increases, the instances of multiple-masking become more common. In any idealized cloud population, such as here considered, when the view angle exceeds a critical value,  $\zeta_c$  illustrated in Figure 3, the value of  $S$  determined by an uncompensating model will be too large, that is,

$$S_j(\zeta) > S(\zeta), \text{ for } \zeta > \zeta_c \quad (8)$$

where the subscript  $j$  indicates apparent cloud cover as specified by any one of the Type A or Type B models in Table 1 and  $S(\zeta)$  is an actual measurement at  $\zeta$ . Allowing  $E(\zeta)$  to be that portion of horizontal area multiply-masked, then for any model  $j$ , the compensated form of the model is

$$S(\zeta) = S_j(\zeta) - E_j(\zeta) \quad (9)$$

where  $E_j(\zeta)=0$  for  $\zeta \leq \zeta_c$ ,  $E_j(\zeta) > 0$  for  $\zeta > \zeta_c$ .

However, cloud cover models employing idealized cloud populations cannot accommodate  $E(\zeta)$  rigorously. As an example, elementary extension of the rectangular solid model in Figure 3 gives

$$E_r(\zeta) = C\beta (\tan \zeta - \tan \zeta_c), \zeta > \zeta_c \quad (10)$$

which when combined with Eq (3) in Eq (9) gives  $S(\zeta) = \text{constant}$ ,  $\zeta > \zeta_c$ .

In real cloud populations each individual cloud has its own  $\zeta_c$  which depends upon its proximity to other clouds and its particular  $\beta$ -value. A cloud cover model based on idealized cloud populations, if it is to be useful, must deal with the combined effects of masking and multiple-masking in a manner which does not compromise the value of the physical quantity  $C$ .

Testing the applicability of any model involves least-squares regression, that is, optimally fitting the model to actual data. Linear regression provides values for two quantities by way of the intercept  $A_0$  and the slope  $A_1$ . The rectangular solid model, Eq (3), becomes  $S_r = A_0 + A_1 \tan \zeta$  where  $A_0 = C$  and  $A_1 = \beta C$ . The sphere model, Eq (2), becomes  $\ln(S_s) = A_0 + A_1 \ln(\sec \zeta)$ , where  $A_0 = \ln C$  and  $A_1$  is expected to be equal to unity. The value of  $C$  cannot be compromised, its evaluation is, after all, a primary objective of

the cloud cover modeling effort. However, the accommodation for multiple-masking can be done through  $A_1$ , specifically through the thickness parameter for Type A models and through the value of the exponent of the  $\zeta$ -function for Type B models. Since  $A_1$  is an exponent for Type B models, it is convenient to replace " $A_1$ " by the simpler symbol " $v$ ". For example, the sphere model expression can be written as  $S_s(\zeta) = C \sec^v \zeta$ .

Determining which cloud cover model best describes the variation in apparent cloud cover with view angle can only be made by comparison with actual  $(\zeta, S)$  data sets. The following section discusses an unique source of such data which is then employed in evaluating these models.

## 5. DATA

A geophysical experiment being conducted during space shuttle missions, the CLOUDS\* experiment, sponsored by the U.S. Air Force, has as a particular objective the collection of high resolution data from various cloud scenes for the quantification of  $S(\zeta)$ . Series of photographs are made of fixed cloud scenes as the orbiting space shuttle passes overhead ( $\zeta \approx 0$ ) and then moves away from them. (Details on the photographic system, films etc. are given in Snow and Tomlinson, 1987.) The entire series, 30 to 40 images, requires less than 4 minutes to complete, thus, the cloud field itself remains unchanged. However, the angle at which any cloud scene is viewed varies through a large portion of its possible range.

Photogrammetric analysis, either manual or computerized, is carried out on these series. The analysis yields values of  $S$  and  $\zeta$  for each photographic image in the series. The manual photogrammetric analysis is performed on 25 x 35 cm prints from the original 35 mm negatives. In the case of computerized analysis, first generation contact negatives are digitized and the values of  $S$  and  $\zeta$  are then determined from the digital imagery. The apparent cloud cover  $S$  is simply

---

\*CLOUDS --- Cloud Logic to Optimize Use of Defense Systems.

the fraction of a fixed area on the Earth's surface which is masked from view, the fraction which is "white" on a positive print. The areas analysed manually are nominally 4000 sq km and those analysed digitally are 2000 to 7000 sq km. The view angle  $\zeta$  is the angle at which the cloud scene is viewed relative to the vertical direction defined at the center of the area analysed. Additional details on photogrammetric analysis are contained in Snow et al, 1985 and on digital image processing in Volfson et al, 1987.

The data from five CLOUDS series are used in this report. All are sub-tropical cloud scenes and all consist of single-layer, opaque, low-based cumuliform clouds. Further details on each series are contained in Table 2. Three images from the BCS series are reproduced in Figure 6. The individual data sets ( $\zeta$ , S) are given later in Table 4 which deals specifically with model application to satellite cloud cover measurements. The number of images analysed from each series in the order given in Table 2 are: 14, 13, 14, 12, 5.

Table 2. Space shuttle CLOUDS photographic series of single-layer cumuliform clouds

Location (Abbreviation)	Approx Latitude ( $^{\circ}$ N)	Area Analyzed (sq km)	Underlying Surface	Mission/ Mo/Yr	Local Solar Time
Baja California Sur, Mexico (BCS)	25	4400	land	51-C/01/85	early afternoon
Cape Canaveral, Florida (CCD)	28	7000	offshore	51-C/01/85	mid-afternoon
Cape Canaveral, Florida (CCH)	28	4500	offshore	51-J/10/85	near noon
Maui, Hawaii (MAU)	21	1700	land	51-C/01/85	near noon
Northeast Dominican Republic (NDR)	19	4000	land	41-D/09/84	late morning

## 6. MODEL TESTING

Any of the cloud cover  $\tau$  can be fitted by the least-squares linear regression method to any of the sets of measurements made from the CLOUDS photographic series. The correlation coefficient is used to quantify a model's ability to reproduce the information contained in a data set.

Linear regressions are performed with the models listed below in: (a) prediction form and (b) regression form. The subscript indicates the model from Section 3 and the ( $\zeta$ ) is understood on the left side of each. The \* indicates a model estimate of the C-value as distinguished from a measurement of C.

$$\text{rectangular solid}\{ \quad S_r = C^* (1 + \beta \tan \zeta) \quad (11a)$$

$$\quad S_r = C^* + \beta C^* \tan \zeta \quad (11b)$$

$$\text{sphere}\{ \quad S_s = C^* \sec^v \zeta \quad (12a)$$

$$\ln (S_s) = \ln C^* + v \ln (\sec \zeta) \quad (12b)$$

$$\text{hemisphere}\{ \quad S_h = C^* (1/2(1 + \sec^v \zeta)) \quad (13a)$$

$$\ln (S_h) = \ln C^* + v \ln (1/2(1 + \sec \zeta)) \quad (13b)$$

$$\text{domed cylinder}\{ \quad S_m = C^* (1/2(1 + \sec \zeta + B \tan \zeta))^v \quad (14a)$$

$$\ln (S_m) = \ln C^* + v \ln (1/2(1 + \sec \zeta + B \tan \zeta)) \quad (14b)$$

In terms of the regression coefficients discussed in Section 4,  $C^* = \ln^{-1}(A_0)$  and  $v \equiv A_1$  is the mechanism used to incorporate the effects of multiple-masking. (The cube, cylinder, ellipsoid and hemi-ellipsoid models are not used because they are either special cases of models used or are obviated by the domed cylinder model.)

Table 3 summarizes the regression results for the five data sets outlined in Table 2. The average values of the correlation coefficient for the first 3 models are: 0.977, 0.984, 0.982. These values indicate that the rectangular solid model overall provides the poorest fit to apparent cloud cover data and the hemisphere model the next poorest fit. The fact that the rectangular solid model does not allow  $dS/d\zeta = 0$  at  $\zeta = 0$  contributes further to its exclusion as a suitable model. The sphere model, Eq (12), in spite of its inflexibility regarding the thickness parameter, provides the best approximation to the data of the first 3 models.

Table 3

## Comparative cloud cover models

## (a) BCS Data Set

	Rectangular Solid	Sphere	Hemi- sphere	Cumuloid
$A_0$	0.3181	-1.0993	-1.0693	-1.1254
$A_1$	0.0719	0.4222	0.6138	0.3738
$C^*$	0.318	0.333	0.343	0.324
$\beta$	0.226	1.000	0.500	---
$v$	---	0.422	0.614	0.374
$r$	0.989	0.989	0.982	0.992

## (b) CCD Data Set

	Rectangular Solid	Sphere	Hemi- sphere	Cumuloid
$A_0$	0.4659	-0.7240	-0.7213	-0.7269
$A_1$	0.1019	0.4365	0.7736	0.3338
$C^*$	0.466	0.485	0.486	0.483
$\beta$	0.219	1.000	0.500	---
$v$	---	0.437	0.774	0.334
$r$	0.924	0.959	0.967	0.951

## (c) CCH Data Set

	Rectangular Solid	Sphere	Hemi- sphere	Cumuloid
$A_0$	0.1174	-1.7235	-1.7038	-1.7454
$A_1$	0.1964	1.4934	2.5805	1.1726
$C^*$	0.117	0.178	0.182	0.175
$\beta$	1.673	1.000	0.500	---
$v$	---	1.493	2.581	1.173
$r$	0.989	0.986	0.984	0.989

Table 3

## Comparative cloud cover models - (Cont)

## (d) MAU Data Set

	Rectangular Solid	Sphere	Hemi- sphere	Cumuloid
$A_0$	0.4196	-0.7735	-0.7642	-0.7838
$A_1$	0.1389	0.5361	0.9213	0.4237
$C^*$	0.420	0.461	0.466	0.457
$\beta$	0.331	1.000	0.500	---
$v$	---	0.536	0.921	0.424
$r$	0.996	0.998	0.996	0.998

## (e) NDR Data Set

	Rectangular Solid	Sphere	Hemi- sphere	Cumuloid
$A_0$	0.2265	-1.3825	-1.3409	-1.4210
$A_1$	0.0870	0.5973	0.8567	0.5338
$C^*$	0.226	0.251	0.262	0.241
$\beta$	0.384	1.000	0.500	---
$v$	---	0.597	0.857	0.534
$r$	0.988	0.990	0.982	0.994

$A_0$  &  $A_1$  - Linear regression coefficients  
 $C^*$  - Cloud cover estimate,  $\ln^{-1}(A_0)$   
 $\beta$  - Thickness parameter  
 $v$  - Exponent, equal to  $A_1$   
 $r$  - Correlation coefficient



Of the Type B models so far considered the domed cylinder model Eq (14) is the first instance where the idealized cloud morphology is not completely defined by the equation, that is, B is not a-priori specified. In order to investigate this cloud cover model it is instructive to assign a value to B which results in a particularly simple expression, specifically  $B = 1$ . (This means that the thickness parameter for the cylindrical portion is  $\beta_c = \pi/8$  and for the entire cloud  $\beta = \pi/8 + 1/2 = 0.893$ ). With  $B = 1$ , it is evident that the domed cylinder model is the linear combination of constant (leading edge),  $\sec \zeta$  (rounded top), and  $\tan \zeta$  (fixed z) portions, see Figure 5.

Other values of B are possible and it is not difficult to design a scheme for determining the value of B for which  $dr/dB = 0$ , that is, the value of B which gives the maximum value of the correlation coefficient r for the model. However, the critical condition that  $dS/d\zeta = 0$  at  $\zeta = 0$  is violated by the domed cylinder model except for: (1) the special case  $B = 0$ , which degenerates Eq (14) back into the hemisphere model, and (2) the condition that B itself is an odd function of  $\zeta$ . If series approximations to the trigonometric functions are substituted into the differentiated form of Eq (14a) two solutions for B are obtained at  $\zeta = 0$ , specifically  $B = 0$  and  $B = [\zeta]$ . Allowing the latter, which is the simplest odd function of  $\zeta$ , the resulting new version of the domed cylinder model is

$$\begin{aligned} \text{cumuloid model} \{ \quad S &= C^* (1/2 (1 + \sec \zeta + \zeta \tan \zeta))^v & (15a) \\ \ln(S) &= \ln C^* + v \ln (1/2(1 + \sec \zeta + \zeta \tan \zeta)) & (15b) \end{aligned}$$

The absence of a subscript on S is deliberate since this cloud cover model will be dealt with almost exclusively throughout the remainder of the report. Whenever S is used hereafter, Eq (15) is implied, unless otherwise stated. This model, referred to as the cumuloid cloud cover model, incorporates certain

necessary conditions, namely its basic morphology, Figure 5, is close to what common experience suggests for cumuliform clouds, and it contains all model characteristics discussed in Section 4.

The results of regression using the cumuloid cloud cover model for the five data sets in Table 3 are provided in the final column. The average value of the correlation coefficients 0.985 is a slight improvement over the next-best sphere model, and only for the CCD data set is the correlation coefficient for the cumuloid model exceeded by any other model. Six images of the CCD cloud field are reproduced in Snow and Tomlinson, 1987. The clouds are stunted cumulus formed under a strong atmospheric inversion. The indication from Table 3(b) is that for these clouds the hemisphere model (no  $\tan\zeta$  term) is most appropriate. However, in general the superior regressions to the CLOUDS data of the cumuloid model, its provision for certain necessary conditions for cloud cover models and its versatility (demonstrated in the following sections) justify its exclusive use.

#### 7. APPLICATION TO SATELLITE CLOUD COVER MEASUREMENTS

In the present development, the regression on any of the five space shuttle data sets has provided the value for the exponent  $\nu$  directly. However, the situation of single measurements ( $\zeta_1, S_1$ ), provided routinely by meteorological satellites, would require an estimation of the value of  $\nu$  if a model such as Eq (15) were to be used to compute C. If the world's cloud populations were categorized by their  $\nu$ -values, then a single measurement would be sufficient to ascertain the cloud cover. Future research might conceivably provide for such an approach but at present such categorization is almost totally lacking.

A second approach is to use two simultaneous measurements,  $(\zeta_1, S_1)$  and  $(\zeta_2, S_2)$ , of basically the same cloud field, for example, from two different meteorological satellites. The determination of  $\nu$  is then straightforward and, once evaluated,  $C$  is calculated from the model equation. For the cumuloid model,  $\nu$  would be computed from

$$\nu = \ln (S_1/S_2) / \ln \left( \frac{1 + \sec \zeta_1 + \zeta_1 \tan \zeta_1}{1 + \sec \zeta_2 + \zeta_2 \tan \zeta_2} \right) \quad (16)$$

A third approach might be to use measurements made at different spectral wavelengths,  $S$  and  $S'$ , but at the same  $\zeta$  to infer  $\nu$ . (In this report the multi-spectral alternative is not pursued further.)

Apart from these speculations, if a model is worth employing, then a large amount of the inherent variation in the phenomenon modeled must be incorporated by the model. In the application being considered, if  $\nu$  changes markedly and unsystematically from one cloud field to another, than such idealized cloud population models are of very limited applicability. The information in Table 3 does contain a wide range of the possible  $\nu$ -values, but a large portion of the variation is explained by the cloud amount itself.

It is reemphasized that  $\nu$  is the mechanism by which multiple-masking is handled in models of form similar to Eq (15). The range of values for the exponent is  $0.0 < \nu < 1.0$ . If multiple-masking does not occur for any values of  $\zeta$ , then  $\nu = 1.0$ , a condition expected for very low  $C$ -values. If multiple-masking is absolutely dominant then  $\nu = 0.0$ , a condition to be approached as  $C$  approaches 1.0. In fact, it may be expected that cloud amount is a physical quantity having considerable effect on the value of  $\nu$ ; when  $C$  is large,  $\nu$  is small and vice versa. The simplest, consistent alternatives are  $\nu \sim (1 - C)$  or  $\nu \sim 1/C$ . From the small sample contained in Table 3, linear regression using the five  $(C, \nu)$  sets for the cumuloid model suggests that  $\nu \sim (1 - C)$  is a somewhat less acceptable approximation than  $\nu \sim 1/C$ , specifically,

$r = 0.79$  for  $v = a(1 - C)^b$  and  $r = 0.88$  for  $v = a/C^b$ . However, the regression coefficients for the second alternative are  $a = 0.15$  and  $b = 1.03$ , or  $b \approx 1$ . This causes the relationship to violate the requirement that  $v$  approaches 1.0 as  $C$  approaches 0.0. In fact, as  $C$  becomes very small,  $v$  then approaches an infinite value. No such violation occurs with the first relationship. The regression coefficient values for the cumuloid model (last column of Table 3) are  $a = 1.16$ ,  $b = 1.94$ . The relationship

$$v = (1 - C)^2 \quad (17)$$

is therefore strongly suggested for the single-layer cumulus clouds analysed. The constraints on  $v$  at the extreme values of  $C$  are met by this expression.

What is needed to provide  $C$ , given a single set  $(\zeta_1, S_1)$  is an expression like Eq (17) along with the model, Eq (15). Introducing Eq (17) into Eq (15b) yields

$$C^* = \ln^{-1}[\ln(S) - (1 - \tilde{C})^2 \ln(1/2(1 + \sec \zeta + \zeta \tan \zeta))] \quad (18)$$

where  $\tilde{C}$  on the right-hand side is an interim value, specifically the previous value of  $C^*$  in the iteration process required to solve Eq (18). When  $C^* = \tilde{C}$ , out to however many decimal places deemed appropriate, then the model estimate for the cloud cover has been obtained.

A definitive evaluation of the cumuloid cloud cover model can only be made by extensive application to other cloud scenes. The formulation of  $v$  may undergo some refinement but the form of Eq (18), whatever the expression for  $v$ , has considerable potential. A preliminary evaluation can be made using the same information which was employed in developing the model. In applying Eq (18) to the data listed in Table 4 and plotted in Figures 7a-7e, the number of iterations for 3 decimal-place precision is approximately 4 for  $\zeta < 50^\circ$  and 8 for  $\zeta > 50^\circ$ . The initial value of  $\tilde{C}$  used to begin the iteration of Eq (18) is the actual measurement of the apparent cloud cover,  $S$ . In Table 4 are contained

TABLE 4

Space shuttle cloud photograph data sets and cloud cover values estimated using cumulo model with  $v = (1-C)^2$ . Comparison value from linear regression on each data set is also included. Negative angle means photo taken on approach to target.

<u>BCS</u>			<u>CCD</u>		
$\zeta$	S	C*	$\zeta$	S	C*
23.5	0.334	0.315	-9.1	0.493	0.491
30.5	0.338	0.305	0.7	0.487	0.487
34.5	0.355	0.312	14.2	0.499	0.493
41.0	0.380	0.317	17.3	0.501	0.492
47.5	0.412	0.324	23.5	0.509	0.493
52.0	0.432	0.322	29.7	0.515	0.488
54.0	0.418	0.308	34.3	0.523	0.487
57.0	0.443	0.304	40.5	0.531	0.479
64.0	0.464	0.268	44.2	0.542	0.479
67.0	0.507	0.279	46.7	0.552	0.482
70.0	0.513	0.246	49.9	0.580	0.502
72.5	0.539	0.233	54.3	0.611	0.520
75.0	0.592	0.234	56.4	0.670	0.589
78.0	0.641	0.204			
Regression Value		0.324	Regression Value		0.483

<u>CCH</u>			<u>MAU</u>		
$\zeta$	S	C*	$\zeta$	S	C*
-49.7	0.337	0.241	17.9	0.476	0.466
-44.2	0.282	0.213	25.5	0.483	0.463
-33.9	0.240	0.203	31.5	0.499	0.468
-25.2	0.211	0.192	35.5	0.513	0.473
-18.3	0.175	0.166	38.0	0.526	0.481
12.9	0.173	0.168	40.4	0.542	0.492
19.3	0.197	0.186	44.1	0.553	0.492
29.0	0.235	0.208	44.6	0.555	0.493
34.6	0.263	0.223	49.2	0.581	0.506
41.8	0.285	0.223	52.4	0.597	0.511
49.4	0.338	0.244	54.4	0.615	0.524
52.5	0.371	0.260	56.7	0.636	0.540
55.4	0.414	0.284			
57.8	0.450	0.305			
Regression Value		0.175	Regression Value		0.457

<u>NDR</u>		
$\zeta$	S	C*
32.0	0.270	0.235
38.0	0.280	0.230
46.0	0.320	0.241
64.0	0.440	0.246
76.0	0.590	0.211
Regression Value		0.241

values of  $C^*$  determined from Eq (18) using the single measurement of  $S$  at each  $\zeta$ -value. The value obtained from linear regression on the entire series with the model, from Table 3, is entered at the bottom of each column for comparison. The extreme departure of any individual value from the regression value is 0.13; most departures are less than 0.05, which is encouraging.

#### 8. APPLICATION TO CLOUD-FREE VIEWING

The probability of having a cloud-free line of sight through the cloudy atmosphere has been studied previously, for example, Lund (1965), McCabe (1965) Lund (1966), Lund & Shanklin (1973), Allen and Malick (1983). These studies have used the most commonly applied measure of cloud amount, specifically sky cover  $N$ , as the parameter in the relationship which estimates the probability of a cloud-free line of sight ( $P_{cflos}$ ) as a function of the elevation angle  $\theta$  above the local horizontal plane. (Note that the term "cloud cover" is often used in cflos publications before 1980 to mean what is herein called "sky cover.") The  $P_{cflos}$  thus obtained is for viewing from a point on the Earth's surface to space, the same geometry used in sky cover determination.

Basically,  $P_{cflos}$  is the complement of the cloudy fraction, specifically unity minus the effect of clouds at any  $\theta$ . (Recall that elevation angle  $\theta = 90^\circ - \zeta$ , see Figure 2.) In the vertical,  $\theta = 90^\circ$ ,  $P_{cflos}(90) = 1 - C$  but at any other  $\theta$ -value the fact that clouds have vertical extent or present a longer cloudy path length must somehow be considered. All previous attempts to quantify this variation have employed statistics determined from the analysis of time series of whole-sky photographs taken at surface locations. However, cloud cover models do precisely what is needed, they quantify apparent cloud cover as a function of view angle using physically realistic cloud morphologies rather than the accumulation of cloud statistics. The cumuloid model is therefore applicable to the cloud-free viewing problem.

In order to have a convenient term to refer to the situation of viewing from space to the Earth's surface, the probability of cloud-free viewing from space

(Pcfvfs) is defined. It is more straightforward than its counterpart Pcflos because the biased estimate for C that sky cover N provides has no effect. Otherwise it is similar; only the direction of view along the line is reversed. (A qualification on this similarity for shallow angle applications is discussed in Appendix B.) Pcfvfs is simply the complement of the apparent cloud cover,

$$Pcfvfs(\theta) = 1 - S(\zeta) \quad (19)$$

where  $\zeta = 90^\circ - \theta$ . Eq (19) is valid for any formulation of apparent cloud cover. For the case of  $S(\zeta)$  given by Eq (15a) and  $v$  given by Eq (17), then Eq (19) is referred to as the cumuloid clear-viewing model, for short, the CMD model.

In Figure 8 the family of probability curves is plotted for the full range of cloud cover values,  $0.0 < C < 1.0$ , in tenths, and in Table 5 the same values of Pcfvfs(%) are listed for every  $10^\circ$  of elevation angle.

Table 5. Probabilities of cloud-free viewing from space (%), Pcfvfs, determined using the cumuloid clear-viewing (CMD) model.

$\theta$ (deg)	Cloud Cover (tenths)										
	0	1	2	3	4	5	6	7	8	9	10
90	100	90	80	70	60	50	40	30	20	10	00
80	100	90	80	70	60	50	40	30	20	10	00
70	100	89	79	69	59	49	39	29	20	10	00
60	100	88	77	67	57	47	38	29	19	10	00
50	100	87	75	64	54	45	36	28	19	10	00
40	100	84	71	60	51	42	34	26	18	09	00
30	100	80	65	54	45	38	31	24	17	09	00
20	100	72	54	43	36	31	26	21	16	09	00
10	100	50	28	20	18	18	17	16	13	08	00

Comparisons are now made between the CMD model and the widely employed cflos models, viz. the SRI formulation by Malick and Allen (1979) of the model originated by Lund and Shanklin in 1973, and the model developed at the Estonian Academy by

Mullamaa, Okhvril and Epik (here referred to as the MOE model), as published in Feigelson (1984). Basically, all such models provide the probability of cloud-free viewing as a function of elevation angle or of local zenith angle using cloud amount as a parameter. (In Appendix A the comparison between the SRI and MOE models is given.)

The SRI formulation uses sky cover  $N$  rather than cloud cover  $C$  for cloud amount and therefore a relationship between  $C$  and  $N$  is needed to carry out the comparison. The relationship proposed by Allen and Malick (1983),

$$C = N/4 + 3N^2/4 \quad (20)$$

is employed to give the following values of  $C$  for each tenth of sky cover over the range  $0.0 \leq N \leq 1.0$ : 0.000, 0.033, 0.080, 0.143, 0.220, 0.313, 0.420, 0.543, 0.680, 0.833, & 1.000. The SRI model, as presented in Malick, Allen, & Zakanycz (1979), is

$$P_{cflos}(\theta) = (1 - C)^\lambda \quad (21)$$

where  $\lambda = 1 + ((0.55 - N/2)/\tan \theta)$  and  $C$  is given by Eq (20). Table 6 contains comparative values of  $P_{cflos}$  and  $P_{cfvfs}$  for each tenth of sky cover and for every  $10^\circ$  of elevation angle. Figure 9 compares the cloud-free probability curves for the CMD and SRI models with cloud cover  $C$  as the parameter. It should be noted that sky cover  $N$  is the cloud amount parameter in Table 6.

At  $C = 6/10$  the probabilities are essentially the same for all view angles. For the smaller view angles,  $\zeta < 45^\circ$  ( $\theta > 45^\circ$ ), there is no significant difference between the models no matter what the cloud amount. However, at the larger view angles, the SRI model gives higher probabilities than the CMD model for clear viewing if  $C < 6/10$  and lower if  $C > 6/10$ . The maximum departures  $\Delta$  are found for small cloud amounts and large view angles (shallow elevation angles), for example, at  $\theta = 10^\circ$ ,  $C = 2/10$ , then  $\Delta = 20\%$ .



The accuracy of either scheme is not assessed here but before using the CMD model at least three facts should be recalled: 1) There were no data for  $C > 5/10$  used in the development of the CMD model and only 6 data points occurred in the region  $\zeta > 65^\circ$  and five of these were from a single data set (refer to Table 4). 2) Only cumuliform clouds were involved in the development of the CMD model, all types were involved in the original data used to develop the SRI model. (Which cloud types were used in the MOE model development is not known.) 3) At shallow elevation angles phenomena which at higher angles have little impact on cloud-free viewing become increasingly significant (refer to Appendix B). Nevertheless, there is the indication that at lower elevation angles (higher view angles) the probabilities presently in use may be optimistic, especially for the smaller amounts of cumuliform cloud cover. More research on situations having both the highest and the lowest cloud amounts is warranted.

Table 6. Probabilities of cloud-free line-of-sight and of cloud-free viewing from space (%),  $P_{cflos}/P_{cfvfs}$ , determined using the SRI model for  $P_{cflos}$  and the cumuloid clear-viewing model for  $P_{cfvfs}$ .

$\theta$ (deg)	Sky Cover (tenths)										
	0	1	2	3	4	5	6	7	8	9	10
90	100/100	97/97	92/92	86/86	78/78	69/69	58/58	46/46	32/32	17/17	01/00
80	99/100	96/97	91/92	85/85	77/78	67/68	57/58	45/45	31/32	16/17	00/00
70	99/100	96/96	91/91	84/85	76/77	66/67	55/57	43/45	30/31	16/16	00/00
60	99/100	96/96	90/89	83/83	74/75	64/66	54/55	42/43	29/31	15/16	00/00
50	99/100	95/95	89/89	81/81	73/72	63/63	52/52	40/41	28/29	14/16	00/00
40	99/100	95/94	88/87	80/78	70/69	60/59	49/49	38/39	26/28	14/15	00/00
30	98/100	94/92	86/83	77/73	67/62	57/53	46/44	35/35	24/26	12/15	00/00
20	98/100	92/89	83/76	72/63	61/52	50/42	40/35	30/29	20/22	10/14	00/00
10	97/100	88/79	74/57	61/38	48/26	36/20	27/18	19/18	12/17	06/12	00/00

The final comparison is made between the CMD Pcfvfs values and Pcflos values generated by the MOE model, which is

$$Pcflos(\theta) = (1 - C) e^{-C(\sec \zeta - 1)b} \quad (24)$$

Here the suggestion made in Ch. 3 of Feigelson (1984) has been followed, specifically  $b = 1.0$ . The cloud amount parameter is  $C$  and therefore these Pcflos values can be compared directly with those in Table 5. In Table 7 and Figure 10 the comparisons are given.

Table 7. Probabilities of cloud-free line-of-sight and of cloud-free viewing from space (%), Pcflos/Pcfvfs, determined using the MOE model for Pcflos and the CMD model for Pcfvfs.

$\theta$ (deg)	Cloud Cover (tenths)										
	0	1	2	3	4	5	6	7	8	9	10
90	100/100	90/90	80/80	70/70	60/60	50/50	40/40	30/30	20/20	10/10	00/00
80	100/100	90/90	80/80	70/70	60/60	50/50	40/40	30/30	20/20	10/10	00/00
70	100/100	89/89	79/79	69/69	58/59	48/49	38/39	29/29	19/20	09/10	00/00
60	100/100	89/88	78/77	67/67	56/57	46/47	36/38	27/29	18/19	09/10	00/00
50	100/100	87/87	75/75	64/64	53/54	43/45	33/36	24/28	16/19	08/10	00/00
40	100/100	85/84	72/71	59/60	48/51	38/42	29/34	20/26	13/18	06/09	00/00
30	100/100	81/80	65/65	52/54	40/45	30/38	22/31	15/24	09/17	04/09	00/00
20	100/100	74/72	54/54	39/43	28/36	19/31	13/26	08/21	04/16	02/09	00/00
10	100/100	56/50	31/28	17/20	09/18	05/18	02/17	01/16	00/13	00/08	00/00

For the small cloud amounts,  $C < 3/10$ , the CMD and MOE results are remarkably similar. However, for  $C > 4/10$  the CMD model systematically gives higher clear-viewing probabilities than the MOE model and the tendency is exacerbated as  $C$  increases. More data at the higher cloud amounts are needed before the discrepancy is finally resolved. In Appendix B phenomenological arguments are made which suggest that an exponential decay with  $C$  and with  $\sec \zeta$ , such as found in the MOE model, should be expected.

## 9. SUMMARY

The high resolution series of cloud photographs taken from the space shuttle are uniquely suited to quantifying the apparent increase in cloud cover as view angle increases. The cumuloid cloud cover model developed from these data may be useful in estimating cloud cover from single measurements of apparent cloud amount made within a visible channel by meteorological satellites. Also, the model furnishes direct evaluation of the probabilities of cloud-free viewing from space. Comparisons between these probabilities and the values given by the two most widely used models for cloud-free line of sight indicate that, over a large range of cloud cover and elevation angle, the cumuloid cloud cover model provides values intermediate between the two.

## REFERENCES

- Allen, J.H., and J.D. Malick, 1983: The frequency of cloud-free viewing intervals. Proc. 21st Aerospace Science Meeting. Am. Inst. Aeron. and Astron., Reno, NV, (January).
- Feigelson, E.M., (Editor), 1984: Radiation in a Cloudy Atmosphere. D. Reidel Publishing Company, Dordrecht, Holland, 293 pp.
- Lund, I.A., 1965: Estimating the probability of clear lines-of-sight from sunshine and cloud cover observations. J. Appl. Meteorol., 4, 714-722.
- Lund, I.A., 1966: Methods for estimating the probability of clear lines-of-sight, or sunshine, through the atmosphere. J. Appl. Meteorol., 5, 625-630.
- Lund, I.A., and M.D. Shanklin, 1973: Universal method for estimating probabilities of CFLOS through the atmosphere. J. Appl. Meteorol., 12, 769-777.
- Malick, J.D., J.H. Allen, and S. Zakanycz, 1979: Calibrated analytical modeling of cloud-free intervals, Proc. Soc. of Photo-Optical Instru. Eng., Vol. 195, Atmospheric Effects on Radiative Transfer, Soc. Photo-Optical Instru. Eng., 142-147.
- McCabe, J. T., 1965: Estimating Mean Cloud Amount and Climatological Probability of Cloud-Free Line-of-Sight. Air Weather Service, USAF, Technical Report 186, Scott AFB, IL, 26 pp.
- Minnis, P., 1989: Viewing zenith angle dependence of cloudiness determined from coincident GOES East and GOES West data. J. Geophys. Res., 74-D2, 2303-2320.
- Snow, J.W., D.D. Grantham, E.M. Tomlinson, and J.H. Willand, 1986. The characterization of cumuliform cloud fields using space shuttle photography, Proc. 2nd Conf. on Sat. Meteorol., Remote Sensing and Applic., Am. Meteorol. Soc., Williamsburg, VA, (May), 228-232.

- Snow, J.W., J.T. Bunting, R.P. d'Entremont, D.D. Grantham, K.R. Hardy, and E.M. Tomlinson, 1985: Space shuttle cloud photographs assist in correcting meteorological satellite data. EOS Trans. Am. Geophys. Union, 66, 489-490.
- Snow, J.W., and E.M. Tomlinson, 1987: Cloud Population Measurements Using Photographs Taken from The Space Shuttle. Preprints 6th Symp. on Meteorol. Obs. and Instru., Am. Meteorol. Soc., New Orleans, LA, (January), 286-289.
- Volfson, L.B., C.T. Peet and C. Gautier, 1987: Initial processing of space shuttle cloud photographs. Air Force Geophysics Laboratory, Hanscom AFB, MA, 64 pp, AFGL-TR-87-0181, ADA183547.

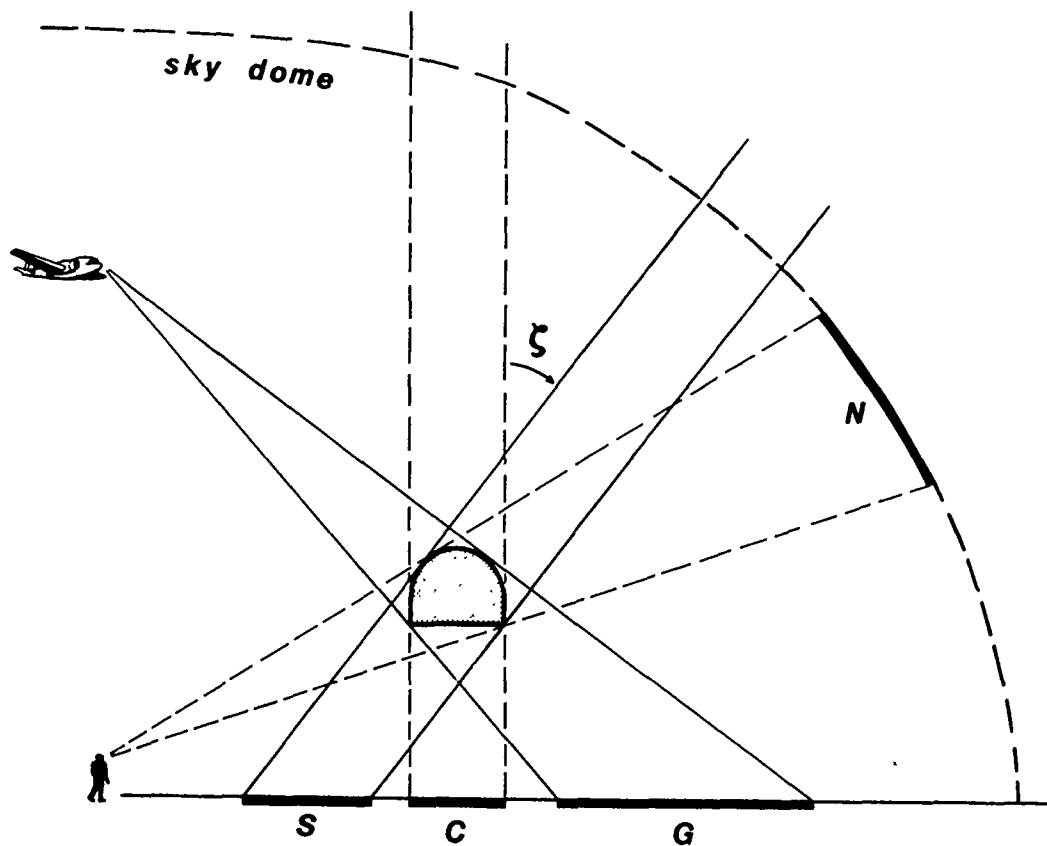


Figure 1. Cloudiness quantifications: S - apparent cloud cover, C - cloud cover, G - ground cover, N - sky cover.  $\zeta$  is view angle. Heavy line segments depict areas masked from view by cloud.

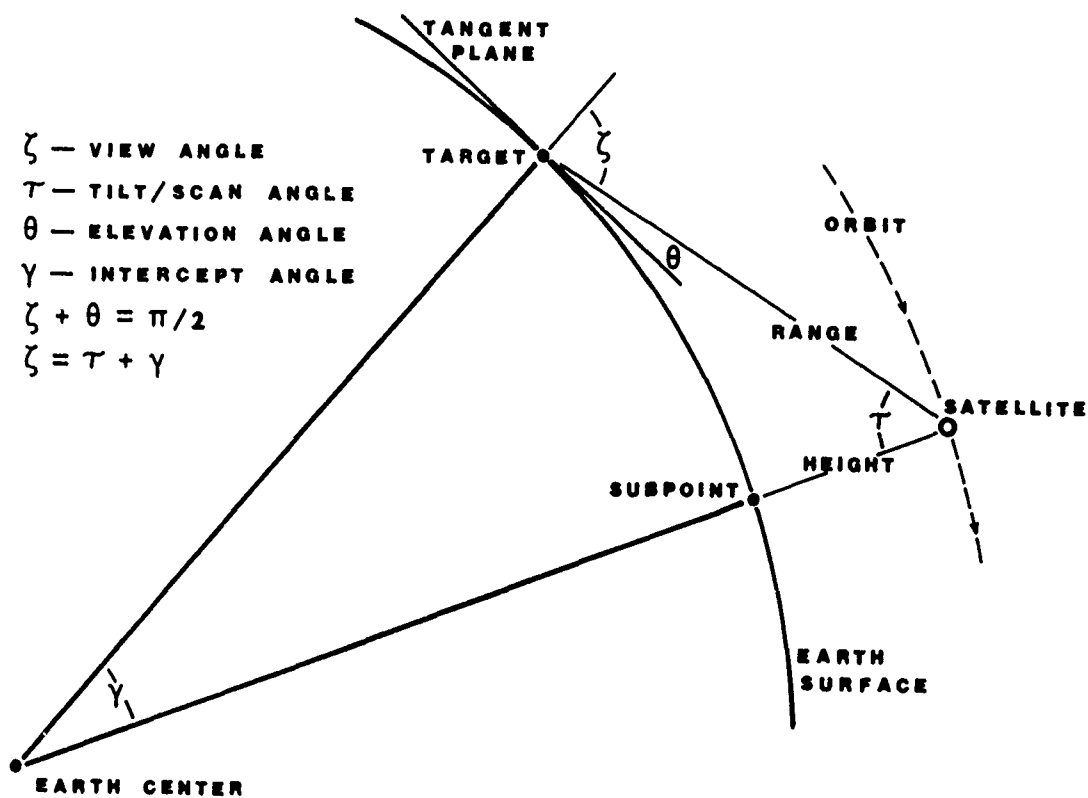


Figure 2. View angle  $\zeta$  and associated elements involved in observing a surface target from an orbital vantage point.

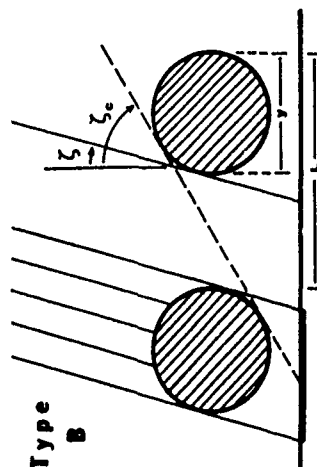
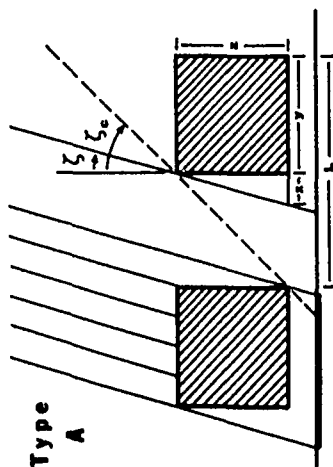


Figure 3. Simple examples of cloud population models, cube for Type A and sphere for Type B, used to derive the apparent cloud cover S as a function of the view angle  $\zeta$ . Heavy horizontal segments signify S. L is recurrence interval, the linear dimension of one complete cycle of cloud/no-cloud.  $\zeta_c$  Cloud cover C is  $y^2/L^2$  for the cube,  $(\pi/4)y^2/L^2$  for sphere.  $S_c = y(y+x)/L^2$ ,  $x = z \tan \zeta$  and  $y = z$  for the cube. Therefore,  $S_c = C(1 + \tan \zeta)$ .  $S_s = (\pi/4)(y^2/L^2) \sec \zeta$ , or  $S_s = C \sec \zeta$ . The critical view angle  $\zeta_c$  is the smallest value of  $\zeta$  for which two clouds mask the same portion of the surface.

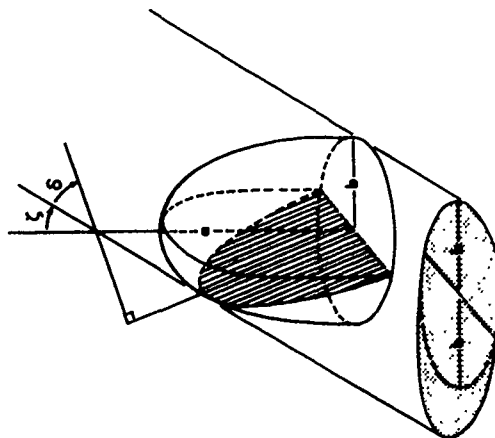
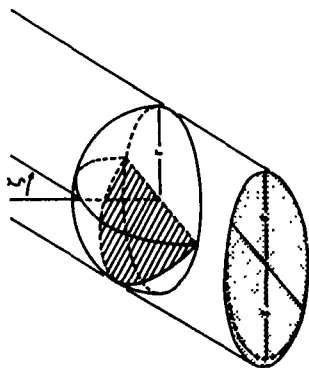


Figure 4. Apparent cloud cover, shaded horizontal areas, resulting from two idealized clouds viewed from angle  $\zeta$ : hemisphere of radius r, hemi-ellipsoid of major axis a and minor axis b. The half toward the direction of view masks as a hemi-disk of radius r or b, respectively. The half away from the direction of view masks as the hatched planes.

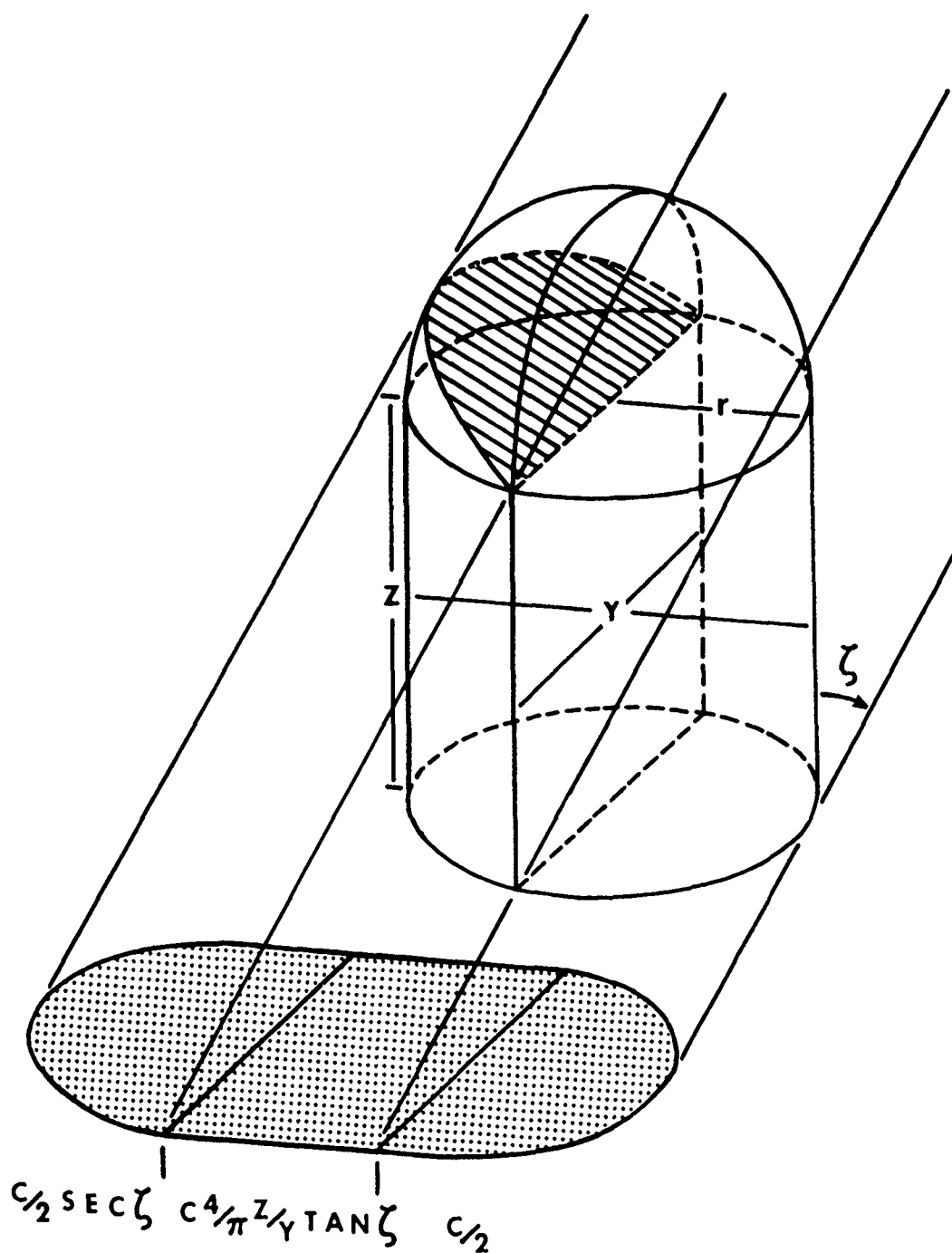


Figure 5. Derivation of the apparent cloud cover for the domed cylinder cloud morphology using the technique of portions. The half toward the direction of view masks as a hemi-disk of radius  $r = y/2$ , the vertical extent of cylinder as a rectangle  $zy$ , and the domed top as the hatched plane. Shaded horizontal area is the total area masked from view,  $C \sim \pi y^2/4$ .



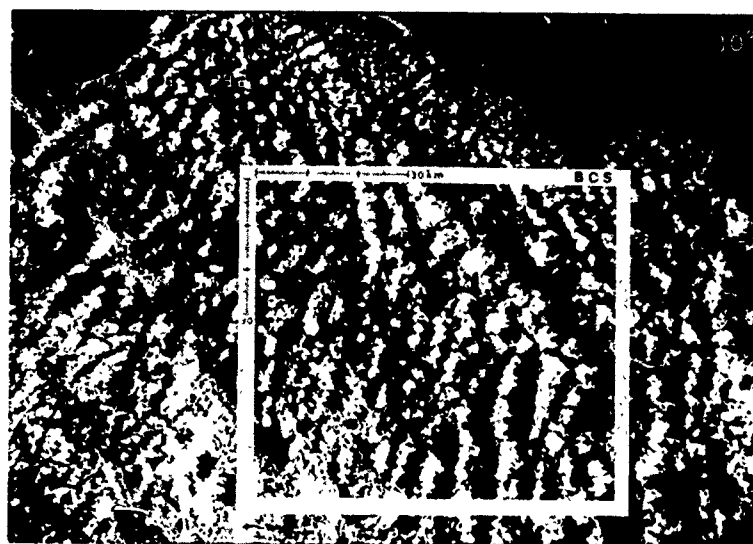
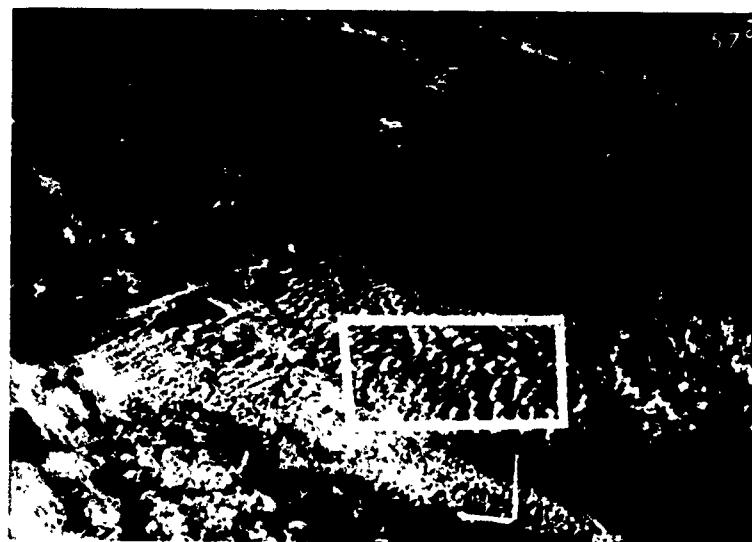
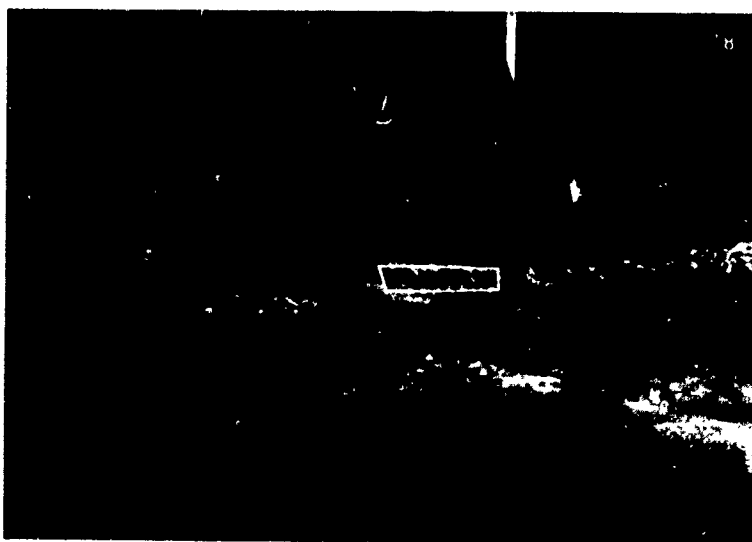
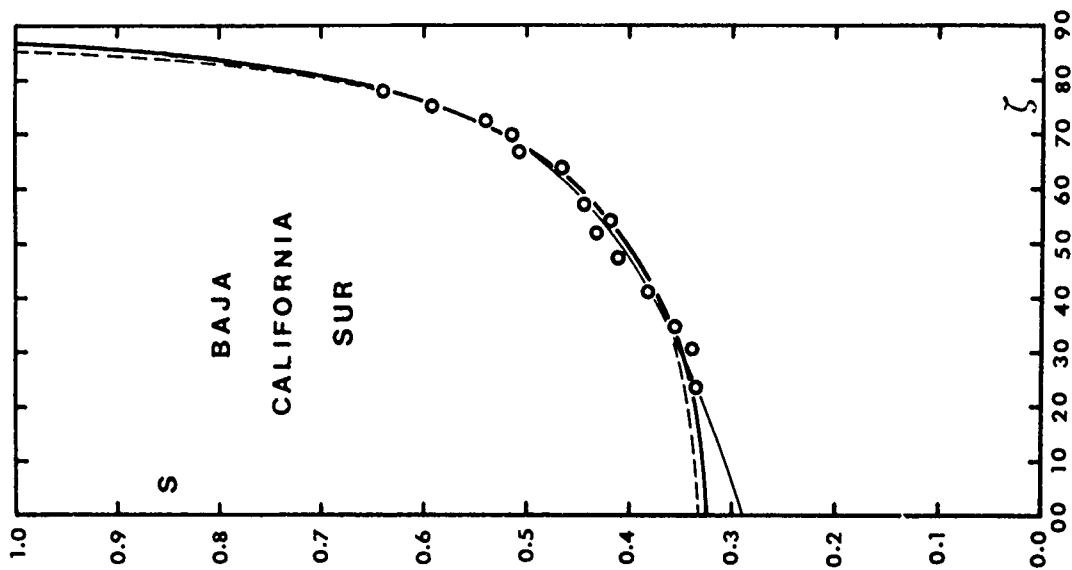
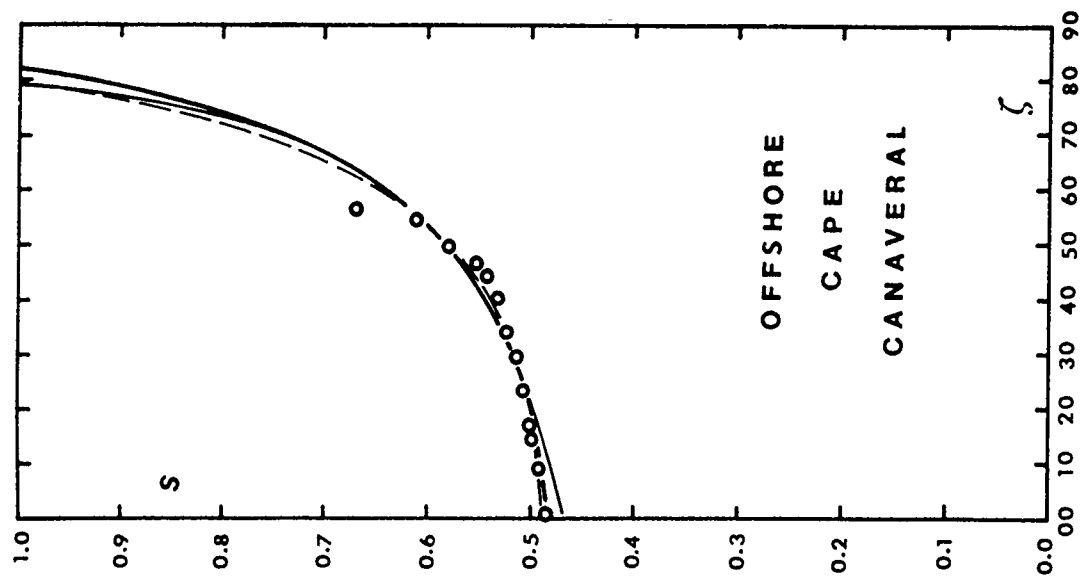


Figure 6. Analysis technique for apparent cloud cover determination. The same area,  $A_{total}$ , is identified in each image (inside edge of white quadrangles) and measurement is made of the portion occupied by clouds,  $A_{cloud}$ . The apparent cloud cover is  $S = A_{cloud}/A_{total}$ . The land is a portion of the state of Baja California Sur, Mexico. The view angle at the center of each of the 3 images is determined photogrammetrically and is shown in the upper right corner. (Inverted numbers, upper left, indicate time.) The photographs were taken by astronaut Gary E. Payton, USAF. Additional details are contained in Table 2.

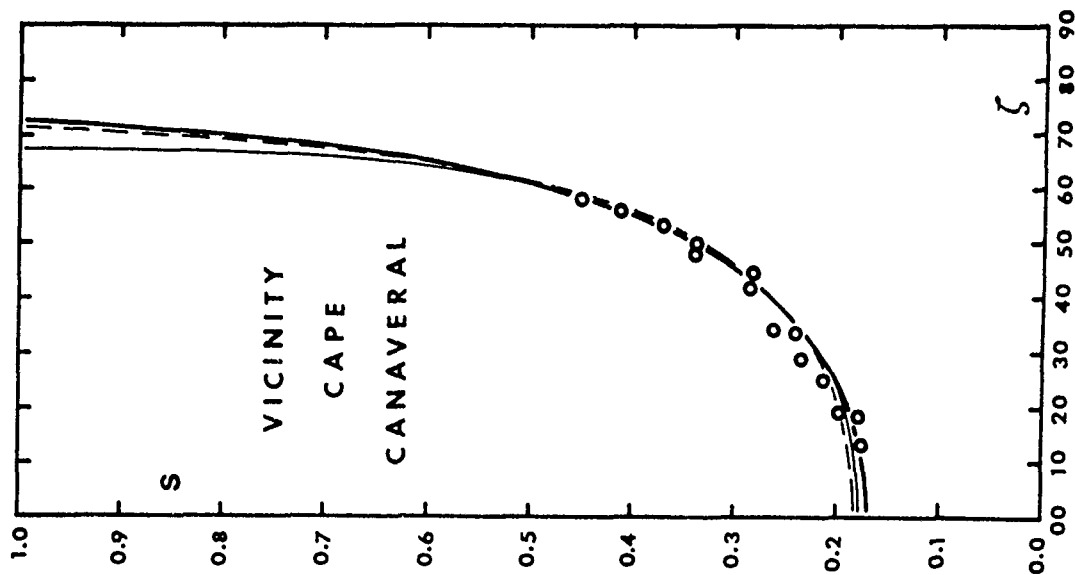
Figure 7. Apparent cloud cover  $S$  as a function of view angle  $\zeta$  for cumuliform clouds. Data from analysis of space shuttle photographs are plotted as open circles. Heavy solid curve is the cumuloïd model Eq (15), light solid curve is the domed cylinder model Eq (14), light broken curve is the sphere model Eq (12).



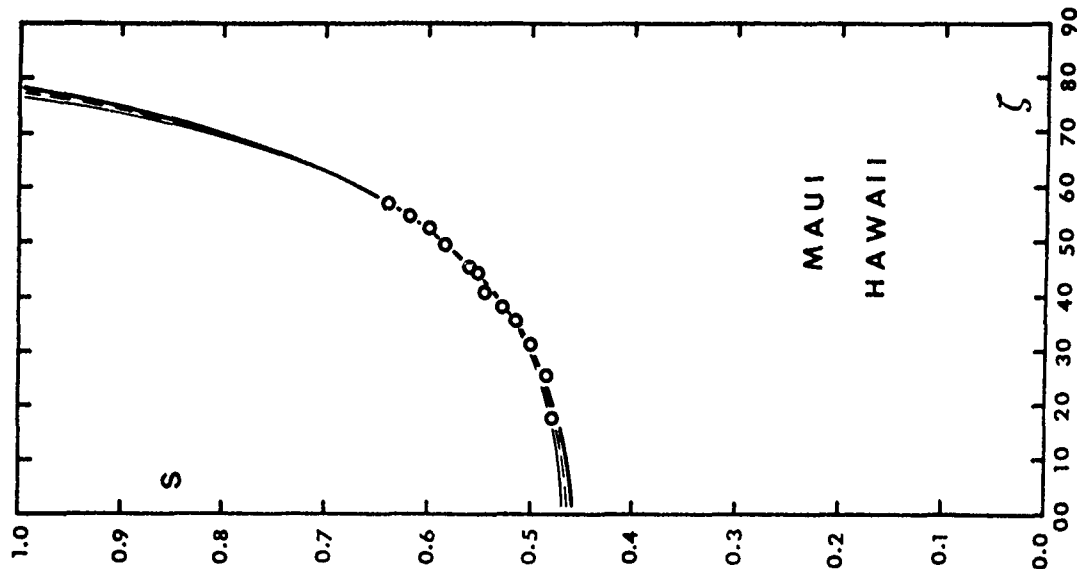
7a. Baja California Sur, Mexico.



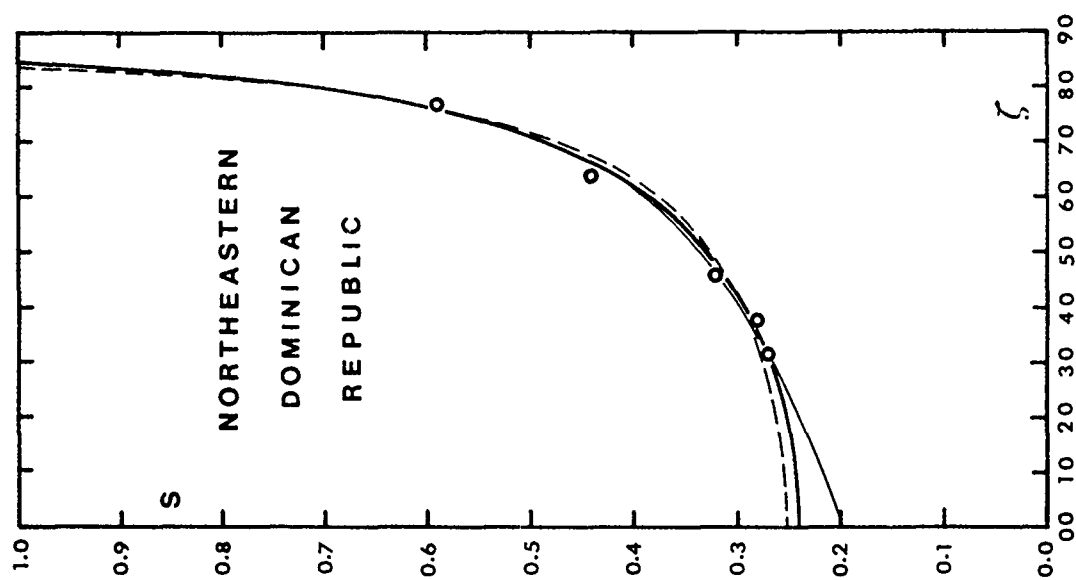
7b. Offshore of Cape Canaveral, Fl.



7c. Vicinity of Cape Canaveral, FL.



7d. Maui, Hawaii.



7e. Northeastern Dominican Republic.

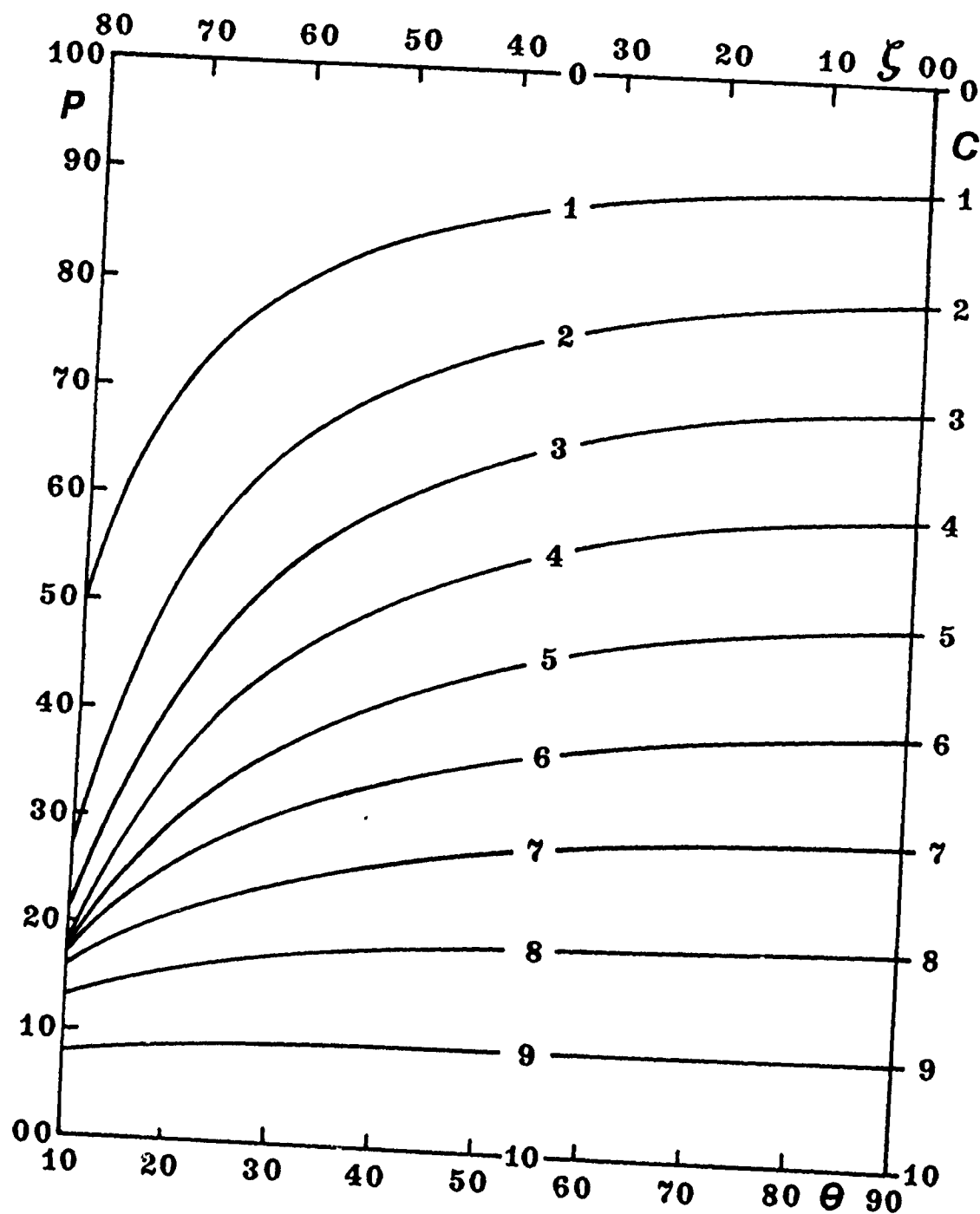


Figure 8. Probability of cloud-free viewing from space  $P(\%)$  as a function of elevation angle  $\theta$  or view angle  $\zeta$  using the cumuloid mode. Cloud cover  $C$  (tenths  $\times 10$ ) is the parameter. Right ordinate expresses  $P(90) = 1 - S(0)$ .

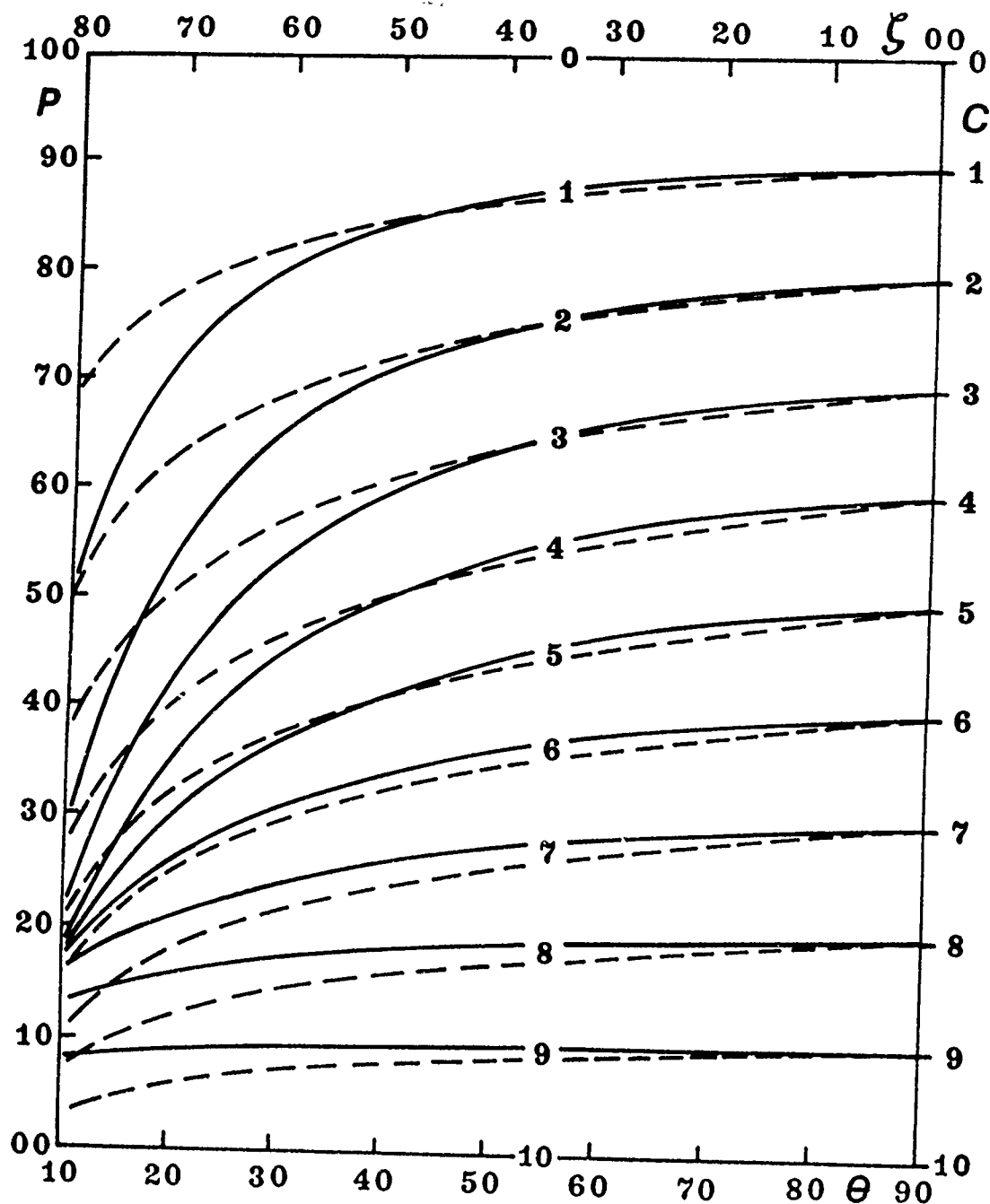


Figure 9. Probability of cloud-free line of sight, cflos - broken curves, and cloud-free viewing from space, cfvfs - solid curves, as functions of elevation angle  $\theta$  or view angle  $\zeta$ . Probability values  $P$  in percent. Cloud cover (tenths  $\times 10$ ) is the parameter. SRI formulation used for cflos and the CMD model used to compute cfvfs values. Conversion from cloud cover to sky cover accomplished using Eq (20). (N-values are given in Appendix A.)

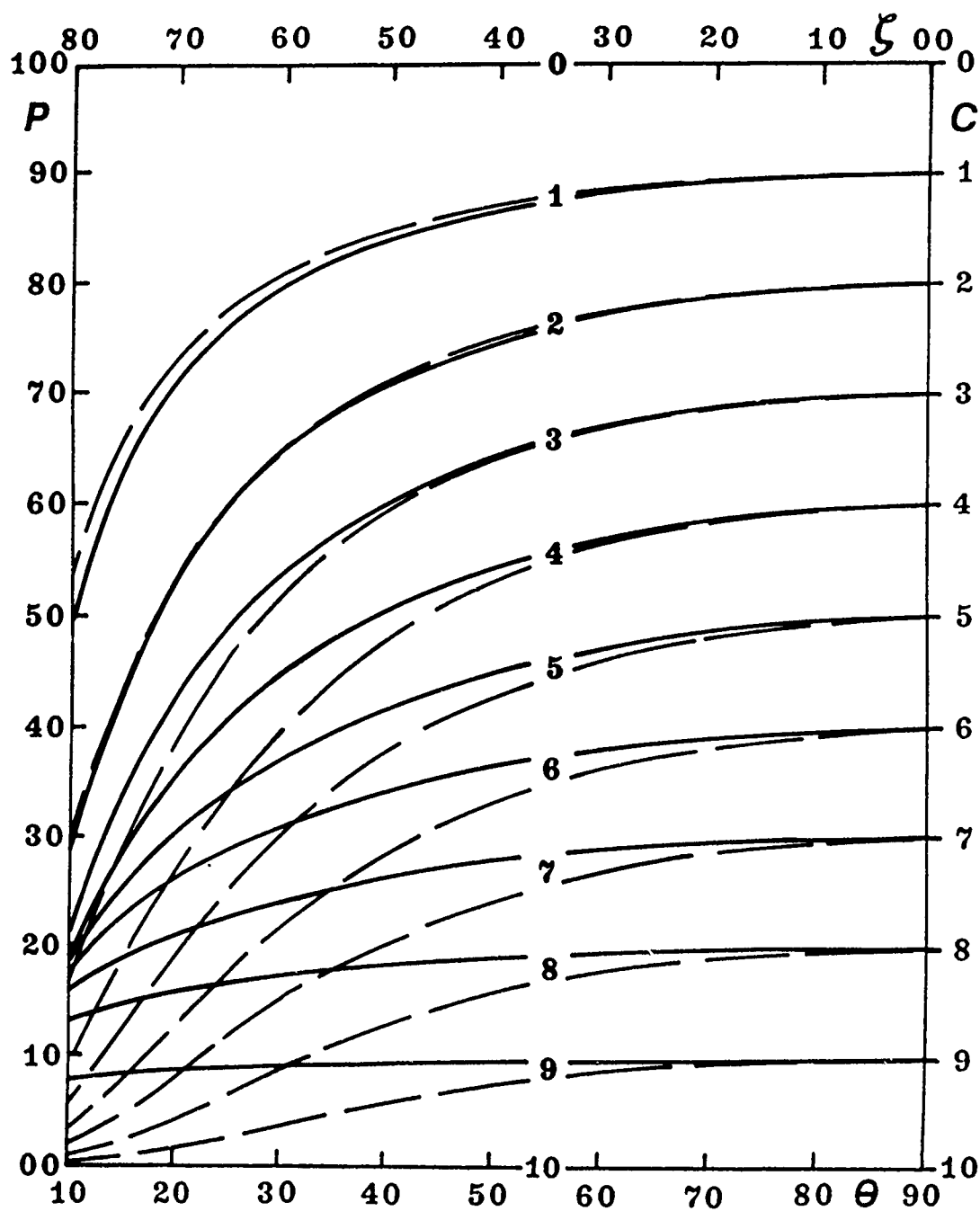


Figure 10. Probability of cloud-free line of sight, cflos - broken curves, and cloud-free viewing from space, cfvfs - solid curves, as functions of elevation angle  $\theta$  or view angle  $\zeta$ . Probability values  $P$  in percent. Cloud cover (tenths  $\times 10$ ) is the parameter. MOE model used for cflos and the CMD model used to compute cfvfs values.

Intentionally Blank

## Intercomparison of the SRI and MOE Pcflos Models

Probability of cloud-free line of sight (Pcflos) models are expressions which specify the likelihood of having an unobstructed line of sight as a function of elevation angle with cloud amount as the parameter. The model which is presently being used in the United States was originally published by Lund and Shanklin (1973) and was refined by Malick, Allen and Zakanycz (1979) from the Stanford Research Institution. Eq (21) of the report is the SRI model. Another Pcflos model, contained in Feigelson (1984), was developed at the Estonian Academy, Tartu, Estonia. This model is Eq (24) and is referred to as the MOE model in the report.

Considerable interest has been expressed in the difference between these two models. For completeness, therefore, Table A and Figure A present the intercomparison. Cloud cover is the parameter. Eq (20) is solved for the following values of sky cover N for each tenth of cloud cover over the range  $0.0 \leq C \leq 1.0$ : 0.000, 0.235 0.376, 0.487, 0.582, 0.667, 0.743, 0.814, 0.879, 0.941, 1.000.

Table A1. Comparative probabilities of cloud-free line of sight determined using the SRI model and the MOE model. Entries are SRI(%) / MOE(%).

$\theta$ (deg)	Cloud Cover (tenths)										
	0	1	2	3	4	5	6	7	8	9	10
90	100/100	90/90	80/80	70/70	60/60	50/50	40/40	30/30	20/20	10/10	00/00
80	100/100	89/90	79/80	69/70	59/60	49/50	39/40	29/30	19/20	10/10	00/00
70	100/100	89/89	78/79	67/69	57/58	47/48	38/38	28/29	19/19	09/09	00/00
60	100/100	88/89	76/78	66/67	56/56	46/46	36/36	27/27	18/18	09/09	00/00
50	100/100	87/87	75/75	64/64	54/53	44/43	35/33	26/24	17/16	09/08	00/00
40	100/100	85/85	73/72	61/59	51/48	42/38	33/29	24/20	16/13	08/06	00/00
30	100/100	83/81	70/65	58/52	48/40	39/30	30/22	22/15	15/09	07/04	00/00
20	100/100	79/74	64/54	52/39	42/28	33/19	26/13	19/08	12/04	06/02	00/00
10	100/100	69/56	51/31	38/17	28/09	21/05	16/02	11/01	07/00	04/00	00/00



Intentionally Blank

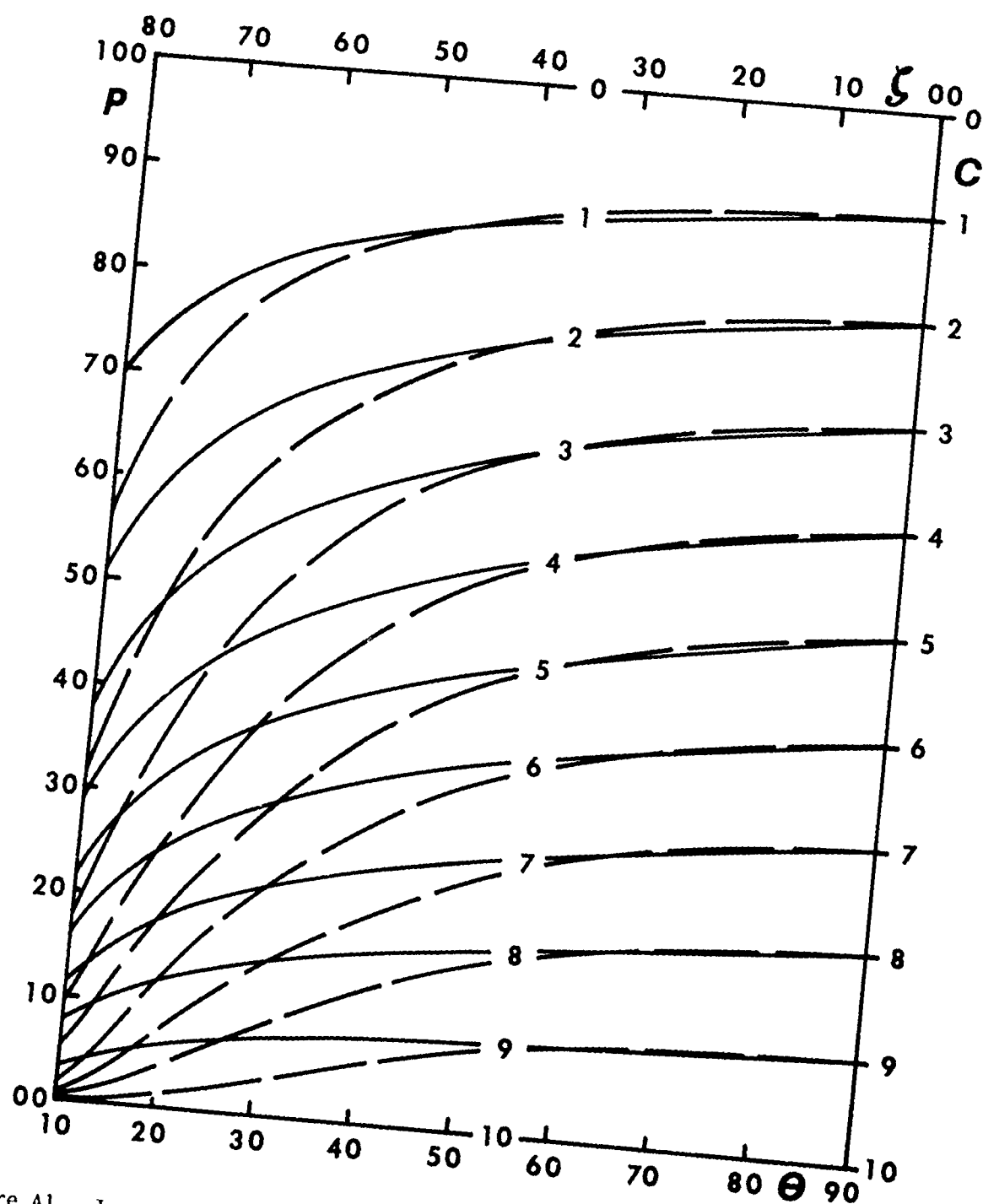


Figure A1. Intercomparison of Pcflos models: solid curves - SRI model (modified Lund/Shanklin), broken curves - MOE model (Malamaa-Okhviril-Epik, also called Eastern European or Russian model).  $P$  is probability in percent,  $\theta$  is elevation angle,  $\zeta$  is view angle,  $\theta + \zeta = \pi/2$ . The cloud amount parameter is cloud cover  $C$  (tenths  $\times 10$ ). At zenith ( $\theta/2$ ),  $P = 10 \times (10-C)$ . Conversion from sky cover to cloud cover accomplished using Eq (20). All curves converge to zero at  $\theta = 0$ .

Intentionally Blank

## APPENDIX B

### Considerations at Shallow-Angles

Very little of the data given in Table 4 is for shallow-angles, specifically, for angles in the range  $\theta < 25^\circ$  ( $\zeta > 65^\circ$ ). The quality of the space shuttle CLOUDS imagery is compromised at these shallow angles because of the great distance between the target clouds and the camera. For example at orbital height of 300km and  $\zeta = 70^\circ$ , the range is 750km, at  $\zeta = 85^\circ$ , 1500 km. Nevertheless, the cumuloid model explains well the data outside of the shallow angle region, specifically  $\zeta < 65^\circ$ , and an initial attempt is made in this appendix to extend clear-viewing probability estimates into the shallow angle region for the low-earth-orbit to surface situation or vice versa. Essentially an heuristic quantification of certain shallow angle phenomena is made and then combined with the results of the cumuloid model.

Factors which have little impact at the lower view angles (higher elevation angles) will become dominant in the shallow angle region (SAR) where viewing is done through a very long atmospheric path. One such factor is the presence of cloud matter which is not totally opaque when viewed near normal. Beyond some angle, this cloud matter obstructs viewing to such an extent that a system, e.g. the human eye, cannot discern the background. This effect is proportional to  $C$  itself since all clouds have some fraction of their total matter which is not opaque. Another factor is multiple scattering within long paths through the atmosphere of light reflected from clouds such that clear lines-of-sight near nadir have reflected light scattered

into them and thereby become cloudy lines-of-sight. Other factors are atmospheric turbidity and reduced resolution of any system's detector as range increases. To conduct a rigorous treatment of these shallow angle phenomena would require the generation of special data sets designed to quantify particular factors.

The increased path length itself must enter into any quantification of the diminishing likelihood of clear viewing in the SAR. The path length through any atmospheric layer of constant vertical thickness  $T$ , at any angle  $\zeta$ , is  $T \sec \zeta$ . The increase in path length from that at nadir is then  $T (\sec \zeta - 1)$ .

A second effect which also increases the path length is the curvative of the Earth and its atmospheric layers. As can be appreciated from Figure 2, this effect is proportional to the intercept angle  $\gamma$ . For any  $\zeta$  the value of  $\gamma$  depends upon the orbital height which, obviously, restricts generality. Further discussion appears below, but at this point the increase in path length due to curvature is proportional to  $\gamma$ .

How increasing path length influences the likelihood of being able to view clearly is in all cases negative, i.e. the longer the path length the smaller the probability of clear viewing. Further the two effects discussed above are independent, the first depending on  $T$  and  $\zeta$ , the second on the radius of the planet essentially. Therefore the change in probability of clear viewing can be expressed as

$$\Delta P_p \sim -\Delta(C\gamma T (\sec \zeta - 1)) \quad (B1)$$

where the subscript  $p$  designates path length effects within a cloudy atmosphere and " $\sim$ " is read "varies with". The baseline

probability of clear viewing through a layer is directly proportional to T, specifically  $P_{p_0} \sim T$  or

$$\frac{\Delta P_p}{P_{p_0}} \sim - \Delta (C\gamma (\sec \zeta - 1)) \quad (B2)$$

which integrates to

$$P_p \sim \exp(C\gamma(1-\sec\zeta)) \quad (B3)$$

The total range of possible values,  $1.0 \geq P_p \geq 0.0$  is covered by this expression for  $0^\circ \leq \zeta \leq 90^\circ$ , as substitution will confirm, for all C and  $\gamma$  values.

Before this expression can be incorporated into a more complete probability of clear viewing model, one more appropriate in the SAR, some generalized specification of  $\gamma$  is needed. Within the low earth orbit (LEO) range, 200 to 600 km, and within the SAR, specifically  $65^\circ < \zeta < 90^\circ$ , the extreme value of  $\gamma$  are  $4^\circ$  and  $24^\circ$ . An average in the SAR and the LEO ranges is  $\gamma = \zeta/7$ . Incorporating this relationship allows an approximation for LEO situations which is a function only of  $\zeta$  specifically

$$P_p \sim \exp(C(\zeta/7)(1-\sec \zeta)) \quad (B4)$$

For an intermediate cloud cover value of  $C=0.5$ , the range of values of this expression is  $0.9 > P_p > 0.0$  within the SAR, and is  $1.0 \geq P_p > 0.9$  within the remaining range,  $0 < \zeta < 65^\circ$ . Thus it is seen that the impact of Eq (B4) is almost totally within the SAR and is very small elsewhere. It is re-emphasized that the above derivation is not rigorous but is consistent and will here be applied to clear viewing assessment for situations of LEO to surface, or vice versa.

The shallow-angle effects expressed in Eq (B4) modulate an otherwise determined probability of cloud-free viewing.

Incorporating Eq (B4) into Eq (19) gives

$$P_{cfvfs}(\theta) = (1-S(\zeta)) \exp(C(\zeta/7)(1-\sec \zeta)) \quad (B5)$$

As in Section 8 of the report, Eq (15a) is used for  $S(\zeta)$  and  $v$  is given by Eq (17). The family of probability curves thus generated is given in Figure B1 and comparisons with the unmodified cumuloid model, the SRI model and the MOE model are presented in Figure B2-B4. For convenience this cumuloid (CMD), shallow-angle region (SAR) clear-viewing model is referred to as the CDS model.

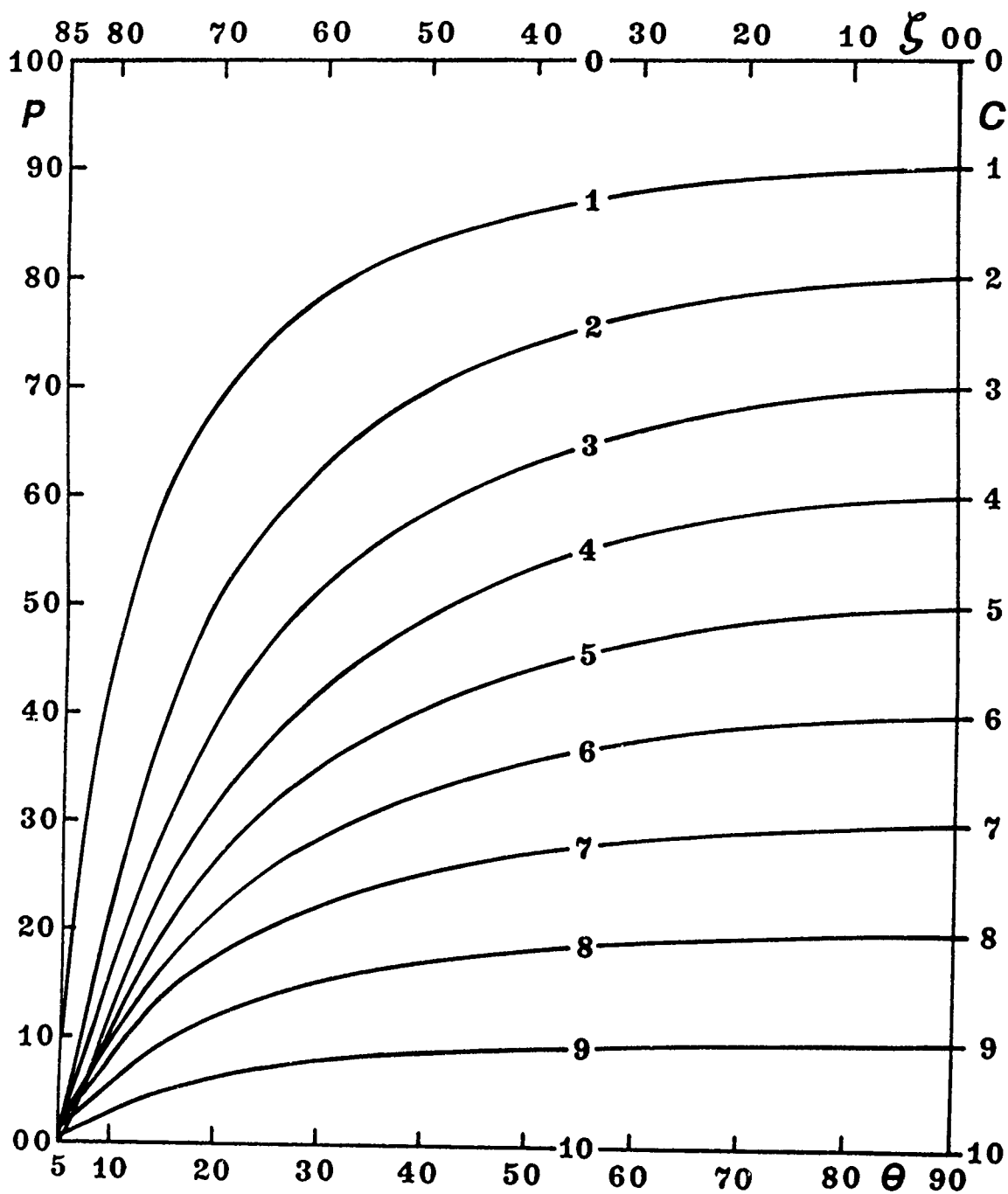


Figure B1. Probability of cloud-free viewing from space (%) as a function of elevation angle  $\theta$  or view angle  $\zeta$  using the cumuloid shallow-angle CDS model. Cloud cover  $C$  (tenths  $\times 10$ ) is the parameter. The right ordinate expresses  $P(90) = 1-S(0)$ .



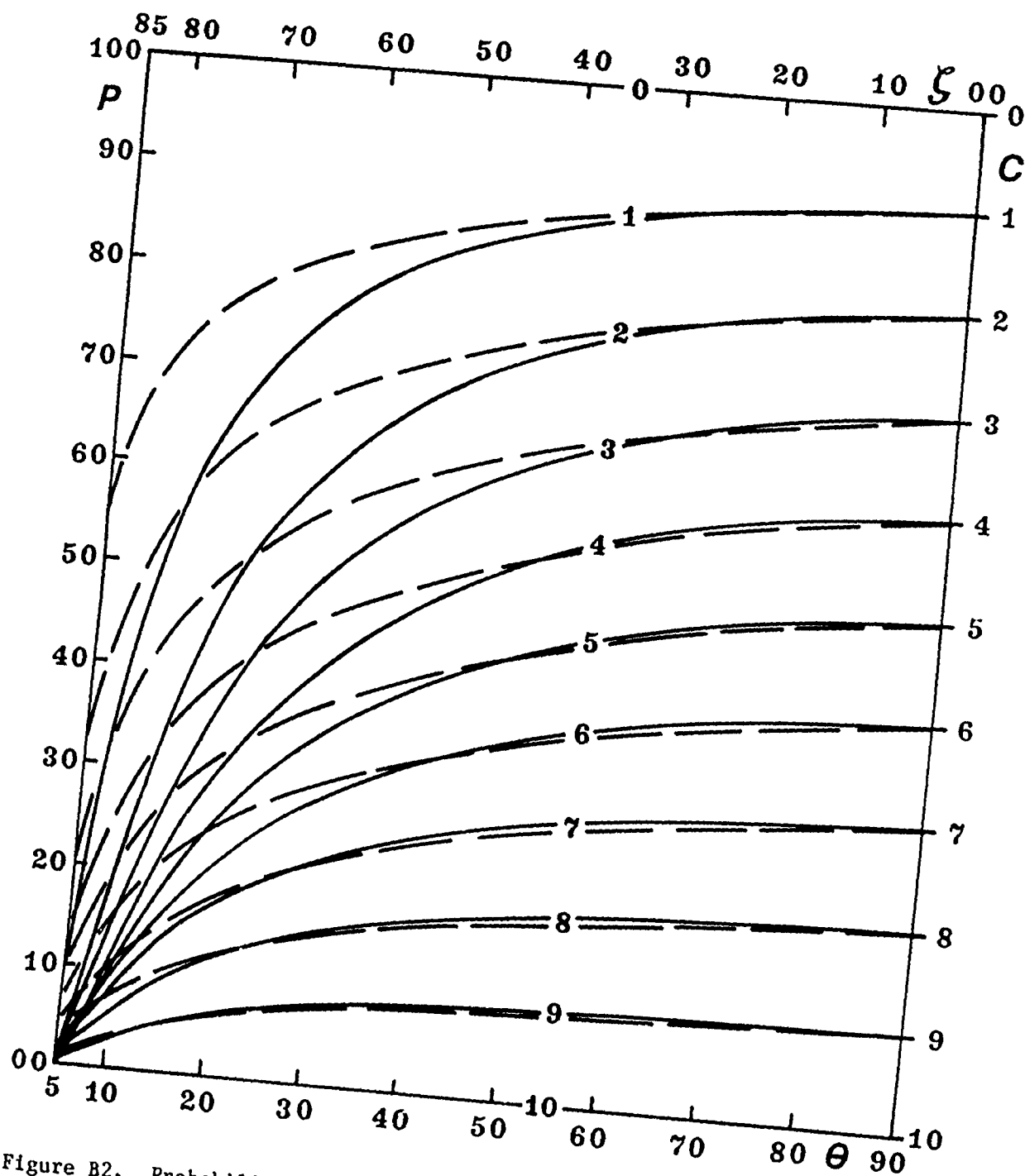


Figure B2. Probability of cloud-free line of sight, cflos - broken curves, and cloud-free viewing from space, cfvfs - solid curves, as function of elevation angle  $\theta$  or view angle  $\zeta$ . Probability values  $P$  in percent. Cloud cover  $C$  (tenths  $\times 10$ ) is the parameter. SRI formulation used for cflos and the CDS model used to compute cfvfs values. Conversion from cloud cover to sky cover accomplished using Eq (20). (See Appendix A for  $N$ -values.)

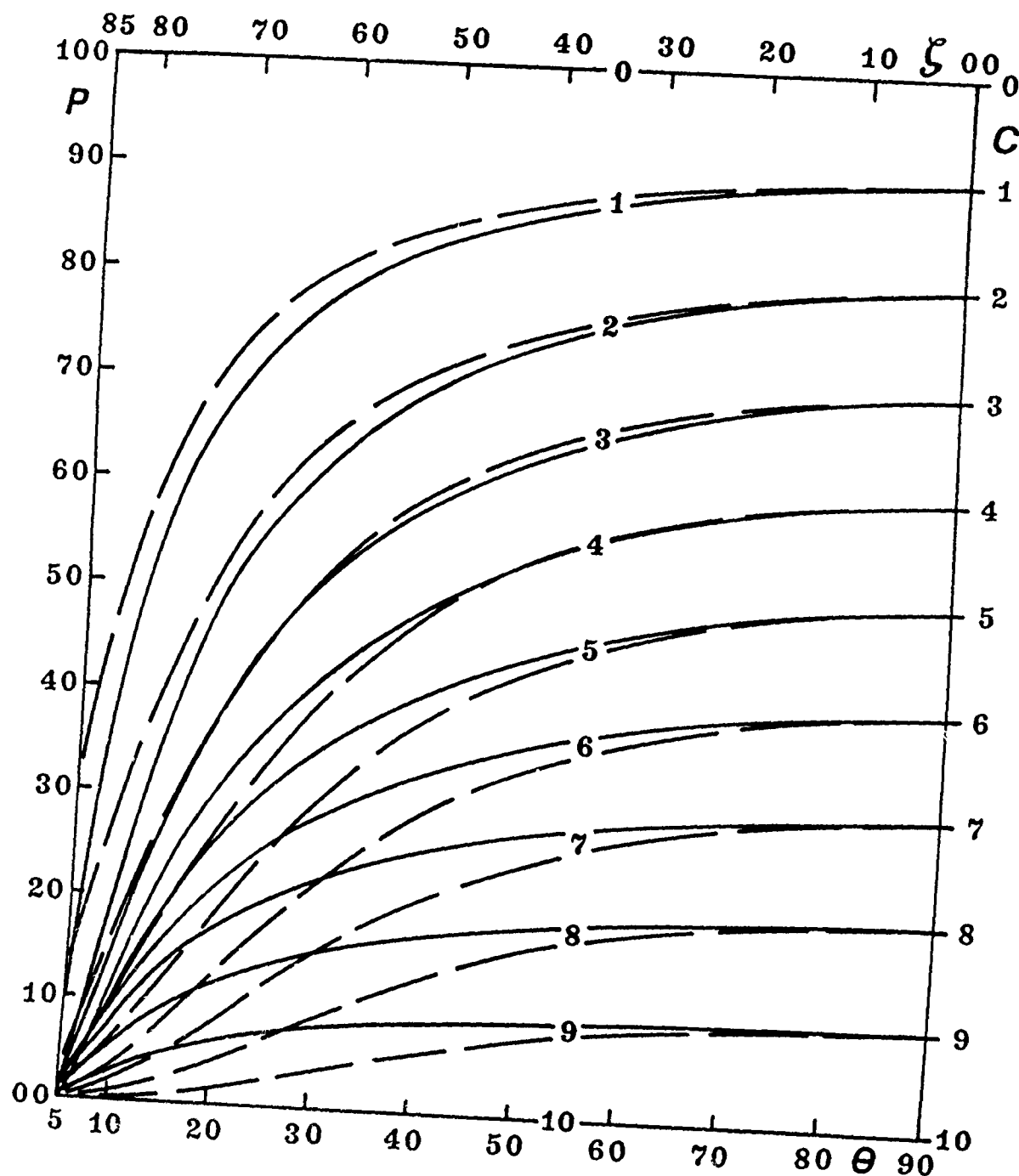


Figure B3. Probability of cloud-free line of sight, cflos - broken curves, and cloud-free viewing from space, cfvfs - solid curves, as functions of elevation angle  $\theta$  or view angle  $\zeta$ . Probability values in percent. Cloud cover  $C$  (tenths  $\times 10$ ) is the parameter. MOE model (see text) used for cflos and CDS model used to compute cfvfs values.

Intentionally Blank